DOI: 10.1002/chem.200700298

Variation of Heterometallic Structural Motifs Based on $[W(CN)_8]^{3-}$ Anions and Mn^{II} Ions as a Function of Synthetic Conditions

Hanhua Zhao, Mikhail Shatruk, Andrey V. Prosvirin, and Kim R. Dunbar*[a]

Abstract: Reactions of $[W(CN)_8]^{3-/4-}$ anions with complexes of Mn^{2+} ion with tridentate organic ligand 2,4,6-tris(2-pyridyl)-1,3,5-triazine (tptz) lead to a series of heterobimetallic complexes. The crystal structures of these compounds are derived from the same basic structural fragment, namely a W_2Mn_2 square constructed of alternating cyanide-bridged W and Mn ions. In $[Mn^{II}(tptz)(OAc)(H_2O)_2]_2\{[Mn^{II}(tptz)(MeOH)_{1.58}(H_2O)_{0.42}]_2[W^{V}(CN)_8]_2\}\cdot 5MeOH\cdot 9.85H_2O$ (**3**), isolated molecular squares are co-crystallized with mononuclear cationic Mn^{II} complexes. The structure of $\{[Mn^{II}(tptz)(MeOH)]_2[W^{IV}(CN)_8]\cdot 2MeOH\}_\infty$ (**4**) is based on an infinite chain of vertex-sharing squares, while $\{[Mn^{II}_2(tptz)_2(MeOH)_3(OAc)][W^{V}(CN)_8]\cdot 3.5MeOH\cdot 0.25H_2O\}_\infty$ (**5**) and $\{[Mn^{II}_2(tptz)_2(MeOH)_3W^{V}(CN)_8][Mn^{II}(tptz)(MeOH)W^{V}(CN)_8]\cdot 2H_2O\cdot MeOH\}_8$ (**7**) are derived from such an infinite chain by removing one of the W-C≡N-Mn linkages in each of the squares. The decanuclear cluster $[Mn^{II}_6(tptz)_6(MeOH)_4(DMF)_2W^{V}_4(CN)_{32}]\cdot 8.2H_2O\cdot 2.3MeOH$ (**6**) is a truncated version of structure **4** and consists of three vertex-sharing W_2Mn_2 squares. The structure of $[Mn^{II}(tptz)(MeOH)(NO_3)]_2[Mn^{II}(tptz)(MeOH)(DMF)]_2[W^{V}(CN)_8]_2\cdot 6MeOH$ (**8**) consists of a hexanuclear cluster, in which the central W_2Mn_2 square is extended by two Mn side-arms attached via CN^- ligands to the W corners of the square. The magnetic behavior of these heterobimetallic complexes (except for **4**) is dominated by antiferromagnetic coupling between Mn^{II} and W^{V} ions mediated by cyanide bridges. Compounds **3**, **6**, and **8** exhibit high spin ground states of S = 4, 13, and 9, respectively, while **5** and **7** exhibit behavior typical of a ferrimagnetic chain with alternating spin centers. Complex **4** contains diamagnetic W^{IV} centers but holds promise as a potential photomagnetic solid.

Keywords: chain structures · crystal structure · cyanides · magnetic properties · molecular squares

Introduction

Stimulated by the discovery of high-temperature Prussian Blue related magnets,[1–3] the field of cyanide-based compounds has rapidly grown into one of the most active areas of coordination chemistry.[4] Over the last decade, research in this area has produced coordination polymers and multinuclear clusters with diverse and interesting properties such as photoinduced magnetism,[5,6] single-molecule magnetism,[7–13] spin crossover,[14–17] and charge transfer induced spin transition.[18,19] With few exceptions, the cyanide containing precursor in the aforementioned chemistry is a homoleptic hexacyanometalate anion. Cyanometalates with coordination numbers other than six have been used much less frequently. It is well known, however, that octacyanometalate anions exhibit facile conversion between three different coordination geometries, namely, the square antiprism, dodecahedron, and bicapped trigonal prism.[20,21] Clearly, the existence of such closely related geometries, with facile interconversion between them, imparts high flexibility to the octacyanometalate building block and confers topological versatility to the multinuclear structures based on these anions.

One of the most intriguing structural types based on the octacyanometalate anions is the family of pentadecanuclear clusters $\{M'[M'^{II}(ROH)_3]_8[M^{V}(CN)_8]_6\}$ obtained from the self-assembly of M'^{II} cations (M′ = Mn, Co, Ni) and $[M^{V}(CN)_8]^{3-}$ anions (M = Mo, W) in ROH (R = Me, Et).[13,22–25] These compounds exhibit high spin ground states, moreover the Co and Ni containing structures were shown to behave as single molecule magnets (SMMs).[13,25] It is also

[a] Dr. H. Zhao, Dr. M. Shatruk, Dr. A. V. Prosvirin, Prof. K. R. Dunbar
Department of Chemistry
Texas A&M University
College Station, Texas 77842-3012
Fax: (+1) 979-845-7177
E-mail: dunbar@mail.chem.tamu.edu

Supporting information for this article is available on the WWW under http://www.chemeurj.org/ or from the author: Additional plots of magnetic data.

worth mentioning that the heptanuclear cluster $[Cu^{II}L]_6[Mo^{IV}(CN)_8](ClO_4)_8$ (L = tris(2-aminoethyl)amine) exhibits interesting photomagnetic behavior based on reversible photoinduced electron transfer between Cu^{II} and Mo^{IV} ions.[6]

Introduction of various blocking ligands directed at limiting the number of available coordinating sites on the M'^{II} ions resulted in a variety of lower dimensional structures with the incorporation of either diamagnetic $[M^{IV}(CN)_8]^{4-}$ or paramagnetic $[M^{V}(CN)_8]^{3-}$ anions.[26,27] An examination of the existing structures revealed, however, that neither of the known compounds contained a trisdentate meridional blocking ligand of the 2,2′:6′,2″-terpyridine (terpy) type. The use of such a blocking ligand would be expected to lead to the formation of new types of heterobimetallic architectures with the incorporation of octacyanometalate anions. For example, the planar tridentate ligand bis(pyridylcarbonyl)amidate ($bpca^-$), when used as a blocking ligand for an octahedral center, produces a structure consisting of the one-dimensional ladder type cationic chain $\{[Fe^{III}(bpca)(CN)_3]Mn^{II}(H_2O)_3\}^+$.[28] Based on these considerations, and our general interest in the study of magnetically coupled cyanide-bridged transition metal ions, we embarked on the preparation of heterometallic complexes by combining $[M(CN)_8]^{n-}$ anions with mononuclear precursors of Mn^{II} ions, with three of the coordination sites in the latter being blocked by the tridentate ligand 2,4,6-tris(2-pyridyl)-1,3,5-triazine (tptz). Herein, we report the first results of this study and discuss the crystal structures and magnetic properties of the compounds obtained to date. It is shown that the use of tptz as a blocking ligand leads to a series of diverse heterobimetallic structures, with the final structure of the complex being dictated by a number of factors, such as the choice of counterion and solvent and the ratio of the reacting metal ions. The most important and interesting observation, however, is that all of the structures are derived from the same basic structural fragment, namely, a cyanide-bridged Mn_2W_2 square. This underlying structural similarity is quite useful for understanding the magnetic properties of the different heterobimetallic molecular complexes and extended phases.

Results and Discussion

Syntheses: Reactions between $[W(CN)_8]^{3-/4-}$ anions and Mn^{II} complexes of the ligand 2,4,6-tris(2-pyridyl)-1,3,5-triazine (tptz) afford a series of cyanide-bridged compounds (Tables 1 and 2) that display structural versatility. The particular extended architecture adopted by these compounds depends on the choice of counterion and solvent, but, importantly, all the structures are characterized by the presence of a common building block, namely, a cyanide-bridged W_2Mn_2 square, or a fragment derived from the square (Scheme 1).

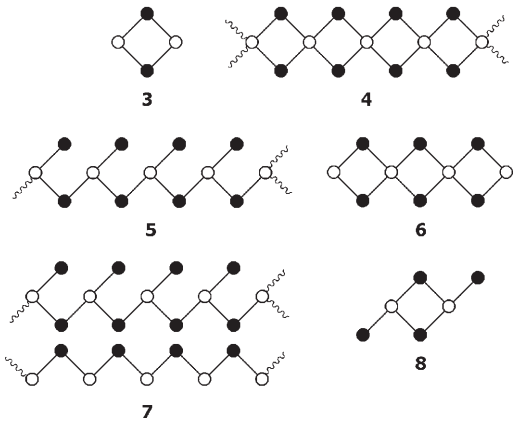

Scheme 1. Schematic representation of the cyanide-bridged transition metal cores in the structures of complexes **3**–**8**. ●: Mn, ○: W.

The reaction that uses $Mn(OAc)_2{\cdot}4H_2O$ and tptz as starting materials yields complex **3**, whose structure consists of a discrete square anion co-crystallized with a mononuclear $[Mn(tptz)(OAc)(H_2O)_2]^+$ cation. The use of the mononuclear precursor **1** results in the decanuclear complex **6** in which three square units are fused together by sharing their W vertices. On the other hand, when complex **2** is used as starting material, the growth of the structure is ceased after two Mn^{II} centers are attached to the central square unit, giving rise to the hexanuclear complex **8**. Interestingly, when $Mn(OAc)_2{\cdot}4H_2O$ and tptz are reacted with a reduced form of the anion, $[W^{IV}(CN)_8]^{4-}$, the square fragment is still preserved: the resulting compound **4** consists of an infinite chain of vertex-sharing squares. Reactions that are carried out in anhydrous solvents lead to complexes **5** and **7**. The structures of these compounds are based on infinite chains which also can be considered as being derived from an infin-

Table 1. Molecular formulas and structures of complexes **1**–**8**.

Complex	Formula	Crystal structure
1	$[Mn(tppz)(MeOH)Cl_2]{\cdot}H_2O$	mononuclear complex
2	$[Mn(tptz)(NO_3)(H_2O)_2](NO_3){\cdot}1.5\,H_2O$	mononuclear complex
3	$[Mn(tptz)(OAc)(H_2O)_2]_2\{[Mn(tptz)(MeOH)_{1.58}(H_2O)_{0.42}]_2[W(CN)_8]_2\}{\cdot}5\,MeOH{\cdot}9.85\,H_2O$	anionic square
4	$\{[Mn^{II}(tptz)(MeOH)]_2[W^{IV}(CN)_8]{\cdot}2\,MeOH\}_\infty$	chain of vertex-sharing squares
5	$\{[Mn_2(tptz)_2(MeOH)_3(OAc)][W(CN)_8]{\cdot}3.5\,MeOH{\cdot}0.25\,H_2O\}_\infty$	chain of vertex-sharing squares with $^1/_4$ of cyanide links broken
6	$[Mn_6(tptz)_6(MeOH)_4(DMF)_2W_4(CN)_{32}]{\cdot}8.2\,H_2O{\cdot}2.3\,MeOH$	three fused vertex-sharing squares
7	$\{[Mn_2(tptz)_2(MeOH)_3W(CN)_8][Mn(tptz)(MeOH)W(CN)_8]{\cdot}2\,H_2O{\cdot}MeOH\}_8$	chain of vertex-sharing squares with $^1/_4$ of cyanide links broken + zigzag chain
8	$[Mn(tptz)(MeOH)(NO_3)]_2[Mn(tptz)(MeOH)(DMF)]_2[W(CN)_8]_2{\cdot}6\,MeOH$	square with two dangling atoms

Table 2. Crystal data and details of the refinement parameters for compounds **1–8**.

	$MnCl_2O_2N_6C_{19}H_{18}$ (**1**)	$MnO_{9.5}N_8C_{18}H_{19}$ (**2**)	$W_2Mn_4O_{26.85}N_{40}C_{100.16}H_{116.02}$ (**3**)	$WMn_2O_4N_{20}C_{48}H_{40}$ (**4**)
space group	$P\bar{1}$ (no. 2)	$P2_1/c$ (no. 14)	$P\bar{1}$ (no. 2)	$C2/c$ (no. 15)
unit cell				
a [Å]	8.675(2)	15.842(3)	15.124(3)	13.212(3)
b [Å]	11.146(2)	12.692(3)	15.507(3)	28.434(6)
c [Å]	12.737(3)	22.927(5)	15.794(3)	13.180(3)
α [°]	104.79(3)		61.28(3)	
β [°]	97.53(3)	96.74(3)	73.86(3)	98.92(3)
γ [°]	105.23(3)		70.57(3)	
V [Å^3]	1122.7(4)	4578(2)	3032(1)	4891(2)
Z	2	8	1	4
ρ_{calcd} [g cm^{-3}]	1.438	1.609	1.584	1.704
μ [mm^{-1}]	0.853	0.647	2.380	2.923
crystal color and habit	yellow block	pale yellow needle	yellow block	blue prism
crystal size [mm]	0.07×0.06×0.02	0.19×0.08×0.05	0.42×0.26×0.17	0.13×0.11×0.08
T [K]	110	150	110	110
radiation, λ [Å]	$Cu_{K\alpha}$, 1.54096	$Mo_{K\alpha}$, 0.71073	$Mo_{K\alpha}$, 0.71073	$Mo_{K\alpha}$, 0.71073
min/max θ [°]	1.69 to 23.39	1.29 to 28.22	1.44 to 28.34	1.43 to 28.30
reflns collected [R_{int}]	8728 [0.083]	27891 [0.074]	19911 [0.029]	15324 [0.039]
independent reflns	3074	10474	13975	5907
data/parameters/restraints	3074/274/0	10474/701/21	13975/857/27	5907/343/0
R [$F_o > 4\sigma(F_o)$]				
R_1	0.085	0.087	0.040	0.024
wR_2	0.234	0.203	0.098	0.057
GoF on F^2	1.014	1.029	1.036	1.033
max/min residual densities [e Å^{-3}]	1.36, −0.68	2.10, −0.81	2.11, −0.96	1.19, −0.92

	$WMn_2O_{8.75}N_{20}C_{52.5}H_{53.5}$ (**5**)	$WMn_2O_{20.5}N_{68}C_{150.3}H_{133.6}$ (**6**)	$W_2Mn_3O_7N_{34}C_{75}H_{60}$ (**7**)	$W_2Mn_4O_{18}N_{44}C_{104}H_{102}$ (**8**)
space group	$P2_1/c$ (no. 14)	$C2/c$ (no. 15)	$P1$ (no. 1)	$P\bar{1}$(no. 2)
unit cell				
a [Å]	14.289(3)	40.18(1)	9.2660(7)	13.299(1)
b [Å]	22.331(4)	14.784(3)	11.7256(9)	13.916(1)
c [Å]	18.852(4)	29.465(6)	21.281(2)	18.714(2)
α [°]			96.007(3)	108.289(1)
β [°]	109.64(3)	97.81(3)	98.903(3)	91.618(1)
γ [°]			111.258(3)	114.672(1)
V [Å^3]	5665(2)	17340(7)	2096.2(3)	2937.0(5)
Z	4	4	1	1
ρ_{calcd} [g cm^{-3}]	1.638	1.641	1.646	1.608
μ [mm^{-1}]	2.538	3.145	3.246	2.451
crystal color and habit	brown block	brown block	brown block	yellow plate
crystal size [mm]	0.16×0.09×0.05	0.19×0.11×0.07	0.27×0.21×0.13	0.26×0.20×0.05
T [K]	110	110	140	140
radiation, λ [Å]	$Mo_{K\alpha}$, 0.71073	$Mo_{K\alpha}$, 0.71073	$Mo_{K\alpha}$, 0.71073	$Mo_{K\alpha}$, 0.71073
min. and max. θ [°]	1.47 to 28.31	1.02 to 28.34	2.41 to 37.28	1.70 to 28.67
reflections collected	36062 [R_{int} = 0.040]	92200 [R_{int} = 0.0479]	59571 [R_{int} = 0.027]	33909 [R_{int} = 0.032]
independent reflections	13489	21116	33782	13673
data/parameters/restraints	13489/763/3	21116/1194/15	33782/1092/6	13673/787/0
R [$F_o > 4\sigma(F_o)$]				
R_1	0.036	0.035	0.028	0.033
wR_2	0.085	0.080	0.074	0.074
GoF on F^2	1.058	1.054	1.061	1.037
maximum and minimum residual densities [e Å^{-3}]	1.27, −1.29	2.06, −1.88	2.11, −1.01	1.78, −0.84

ite chain of vertex-sharing squares of **4** upon breaking one of the W-C≡N-Mn bridges in each of the squares. The chain structure of **5** is neutral whereas the chain in **7** is positively charged and co-crystallizes with a negatively charged chain that consists of alternating Mn and W centers bridged by cyanide ligands.

Crystal structures

$[Mn(tppz)(MeOH)Cl_2]\cdot H_2O$ (1) and $[Mn(tptz)(NO_3)(H_2O)_2](NO_3)\cdot 1.5\,H_2O$ (2): Compound **1** is a mononuclear Mn^{II} complex whose coordination environment consists of a tridentate tptz ligand, two chloride ions, and a MeOH solvent molecule (Figure 1a). The Cl^- ligands are arranged in a *cis* disposition with respect to each other, with one of them being *trans* to a central N atom of the tptz ligand and the other being opposite to the MeOH molecule. In the crystal structure of **2**, the Mn^{II} center adopts a heptacoordinate environment of a pentagonal bipyramid, with the equatorial plane including a tridentate tptz ligand and a bidentate NO_3^- anion and the axial positions being occupied by two water molecules (Figure 1b). The Mn–N distances to the coordinated nitrogen atoms of the tptz molecule and the N-Mn-N bite angle measured with respect to the coordinating pyridyl nitrogen atoms are similar in both structures (Table 3).

$[Mn(tptz)(OAc)(H_2O)_2]_2\{[Mn(tptz)(MeOH)_{1.58}(H_2O)_{0.42}]_2[W(CN)_8]_2\}\cdot 5\,MeOH\cdot 9.85\,H_2O$ (3): The crystal structure of **3** consists of an anionic molecular square, $\{[Mn(tptz)(MeOH)_{1.6}(H_2O)_{0.4}]_2[W^V(CN)_8]_2\}^{1-}$, that is co-crystallized with another tptz-containing moiety, namely the $[Mn^{II}(tptz)(OAc)(H_2O)]^{1+}$ cation (Figure 2a). The hepta-

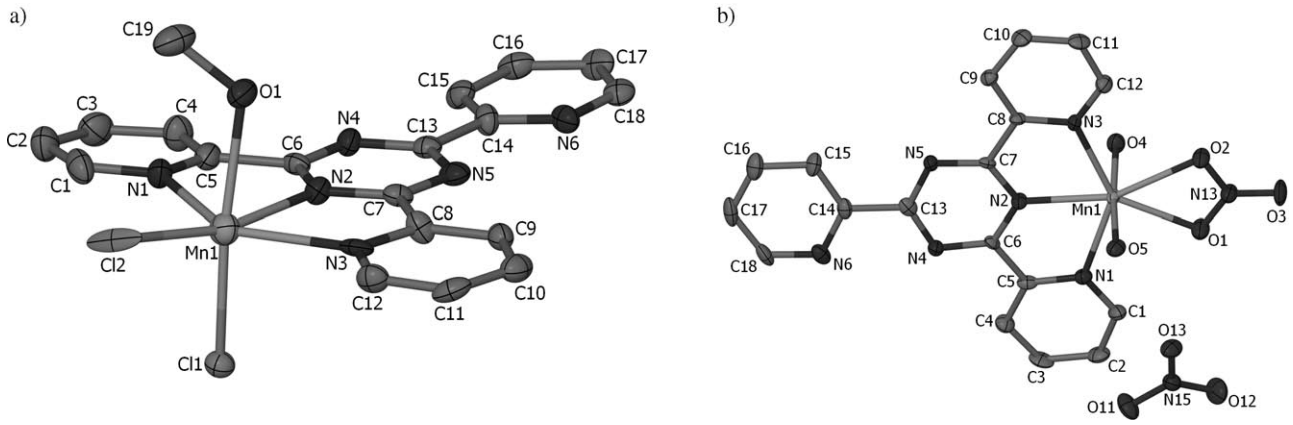

Figure 1. Molecular drawings from the crystal structures of the mononuclear complexes a) **1** and b) **2** (thermal ellipsoids at the 50% probability level; H atoms and solvent molecules are omitted for the sake of clarity).

Table 3. Selected bond lengths [Å] and angles [°] for **1** and **2**.

		1	
Mn1–N1	2.348(7)	N1-Mn1-N3	140.4(2)
Mn1–N2	2.237(6)	N1-Mn1-N2	70.6(2)
Mn1–N3	2.366(7)	N2-Mn1-N3	70.1(2)
Mn1–Cl1	2.434(3)	Cl1-Mn1-Cl2	100.77(9)
Mn1–Cl2	2.452(2)		
Mn1–O1	2.326(6)		
		2	
Mn1–N1	2.367(3)	N1-Mn1-N3	139.4(1)
Mn1–N2	2.230(3)	N1-Mn1-N2	69.5(1)
Mn1–N3	2.349(3)	N2-Mn1-N3	70.0(1)
Mn1–O1	2.304(3)	O1-Mn1-O2	54.84(9)
Mn1–O2	2.370(3)	O4-Mn1-O5	175.6(1)
Mn1–O4	2.154(3)		
Mn1–O5	2.192(3)		

coordinate environment of the Mn2 site in the mononuclear cation resembles the coordination of the Mn1 site in the crystal structure of **2**. The equatorial plane of the pentagonal bipyramid is composed of a tridentate tptz ligand and a bidentate OAc^- anion, and the axial sites are occupied by two water molecules. Interestingly, the Mn^{II} ions at the corners of the square also exhibit a heptacoordinate geometry in the form of a pentagonal bipyramid. One axial position is occupied by a bridging CN^- ligand, while the other axial site is disordered and occupied almost equally by an MeOH and an H_2O molecule. The five equatorial sites are coordinated to a tridentate tptz molecule, a second bridging CN^- ligand, and an MeOH solvent molecule. The axial Mn1–O6 and Mn1–N5 distances (2.145(3) and 2.157(3) Å, respectively) are much shorter than the corresponding equatorial distances Mn1–O7 and Mn1–N (2.455(4) and 2.222(4)–2.499(4) Å, respectively), a reflection of the increased steric crowding in the equatorial plane. The W1 center is in a square antiprismatic coordination environment composed of two bridging and six terminal CN^- ligands. The molecular square is distorted and best described as a rhombus, the distortion being most easily observed by the deviation of the N5-Mn1-N8 and C5-W1-C8 angles from the value of 90° expected for an ideal square geometry (Table 4).

The intermolecular interactions in the crystal structure of **3** are dominated by hydrogen bonding and intermolecular π–π contacts between tptz ligands. The squares form stacks along the *c* axis (Figure 2b), and the mononuclear cations are arranged between the stacks. The tptz ligands form intermolecular π–π contacts between the cations, the squares, and also between cations and squares.

Interestingly, discrete molecular squares have been rarely observed in bimetallic assemblies based on the octacyanotungstate or octacyanomolybdate anion. To our knowledge, the compound $K_2\{[Co^{III}(tren)]_2[W^{IV}(CN)_8]_2\}\cdot 9H_2O$ reported by Kania et al.[29] is the only example of such a structure, in which the Co_2W_2 squares are interconnected through K^+ ions into a layered structure by means of K-N≡C interactions with the terminal cyanide groups. Compound **3**, therefore, represents the first structurally characterized example of a discrete magnetic molecular square based on the $[W^V(CN)_8]^{3-}$ building block.

$\{[Mn^{II}(tptz)(MeOH)]_2[W^{IV}(CN)_8]\cdot 2MeOH\}_\infty$ (4): The crystal structure of **4** contains a square fragment similar to that observed in **3**. In the structure of **4**, however, the square fragments are interconnected through shared W vertices to form an infinite chain of squares (Scheme 1). Another difference is that Mn^{II} ions in **4** are in a distorted octahedral environment that consists of one tridentate tptz ligand, two bridging CN^- ligands, and one MeOH molecule (Figure 3a). The decrease in the coordination number of the Mn centers as compared to **3** is reflected in the closer approach of the N atoms of the bridging cyanides (2.127(2) and 2.151(2) Å) as compared to the distances observed in **3** (2.157(3) and 2.222(4) Å). The $[W^{IV}(CN)_8]^{4-}$ anion is in a square antiprismatic conformation, with four bridging and four terminal CN^- ligands. The W1 center is situated on a two-fold rotation axis and connects two adjacent squares, thus resulting in a chain of vertex-sharing squares.

Table 4. Selected bond lengths [Å] and angles [°] for compounds **3**–**8**.

3			
Mn1−N5	2.157(3)	N5-Mn1-N8	96.7(1)
Mn1−N8	2.222(4)	N9-Mn1-N11	134.2(1)
Mn1−N9	2.499(4)	N9-Mn1-N10	67.0(1)
Mn1−N10	2.317(3)	N10-Mn1-N11	68.2(1)
Mn1−N11	2.420(4)	O6-Mn1-N8	84.7(1)
Mn1−O6	2.145(3)	Mn1-N5-C5	156.6(3)
Mn1−O7	2.455(4)	Mn1-N8-C8	169.3(3)
Mn2−N15	2.356(3)	N15-Mn2-N17	137.7(1)
Mn2−N16	2.265(3)	N15-Mn2-N16	69.1(1)
Mn2−N17	2.401(3)	N16-Mn2-N17	69.0(1)
Mn2−O2	2.252(3)	O2-Mn2-O3	56.8(1)
Mn2−O3	2.322(3)	O4-Mn2-O5	174.4(1)
Mn2−O4	2.172(3)	O4-Mn2-N15	84.2(1)
Mn2−O5	2.181(3)	O4-Mn2-N17	86.9(1)
W1−C8	2.157(4)	W1-C5-N5	178.5(4)
W5−C5	2.164(4)	C5-W1-C8	71.8(2)
C5−N5	1.134(5)	W1-C8-N8	176.2(4)
C8−N8	1.135(5)		
4			
Mn1−N2	2.151(2)	N5-Mn1-N7	139.79(7)
Mn1−N4	2.127(2)	N5-Mn1-N6	70.24(7)
Mn1−N5	2.351(2)	N6-Mn1-N7	70.06(7)
Mn1−N6	2.226(2)	O1-Mn1-N2	165.99(7)
Mn1−N7	2.344(2)	N2-Mn1-N6	99.71(8)
Mn1−O1	2.270(2)	Mn1-N4-C4	173.0(2)
W1−C2	2.151(3)	C2-W1-C4	177.0(2)
W1−C4	2.165(2)	W1-C2-N2	177.0(2)
C2−N2	1.149(3)	W1-C4-N4	177.9(2)
C4−N4	1.154(3)		
5			
Mn1−N9	2.357(3)	N9-Mn1-N11	138.1(1)
Mn1−N10	2.267(3)	N9-Mn1-N10	69.3(1)
Mn1−N11	2.375(3)	N10-Mn1-N11	68.9(1)
Mn1−N2	2.224(3)	N2-Mn1-N10	87.2(1)
Mn1−O1	2.325(3)	N2-Mn1-O3	170.7(1)
Mn1−O2	2.236(3)	O1-Mn1-O2	57.4(1)
Mn1−O3	2.225(3)	Mn1-N2-C2	142.8(3)
Mn2−N1	2.203(3)	N15-Mn2-N17	136.1(1)
Mn2−N5	2.232(3)	N15-Mn2-N16	68.1(1)
Mn2−N15	2.434(3)	N16-Mn2-N17	69.1(1)
Mn2−N16	2.286(3)	N1-Mn2-N5	106.4(1)
Mn2−N17	2.357(3)	O4-Mn2-O5	124.6(1)
Mn2−O4	2.415(3)	Mn2-N1-C1	166.4(3)
Mn2−O5	2.256(3)	Mn2-N5-C5	158.5(3)
W1−C1	2.185(4)	C1-W1-C2	72.0(1)
W1−C2	2.158(4)	C1-W1-C5	142.2(1)
W1−C5	2.153(4)	W1-C1-N1	176.6(3)
C1−N1	1.137(5)	W1-C2-N2	176.9(3)
C2−N2	1.152(5)	W1-C5-N5	175.2(3)
C5−N5	1.145(5)		
6			
Mn1−N1	2.298(4)	N17-Mn1-N19	133.0(1)
Mn1−N9	2.308(4)	N17-Mn1-N18	66.4(1)
Mn1−N17	2.511(4)	N18-Mn1-N19	67.2(1)
Mn1−N18	2.361(4)	O1-Mn1-O2	169.0(1)
Mn1−N19	2.502(4)	N1-Mn1-N9	80.4(1)
Mn1−O1	2.199(3)	Mn1-N1-C1	175.8(4)
Mn1−O2	2.179(3)	Mn1-N9-C9	167.6(4)
Mn2−N3	2.217(4)	N23-Mn2-N25	142.0(1)
Mn2−N10	2.103(6)	N23-Mn2-N24	71.1(2)
Mn2−N23	2.329(4)	N24-Mn2-N25	71.4(2)
Mn2−N24	2.186(4)	N3-Mn2-O5	176.2(2)
Mn2−N25	2.289(5)	N3-Mn2-N10	87.8(2)

Table 4. (Continued)

6			
Mn2−O5	2.151(4)	Mn2-N3-C3	158.1(4)
		Mn2-N10-C10	172.9(8)
Mn3−N2	2.252(4)	N29-Mn3-N31	132.7(1)
Mn3−N4	2.190(4)	N29-Mn3-N30	68.2(1)
Mn3−N29	2.425(4)	N30-Mn3-N31	66.1(1)
Mn3−N30	2.323(3)	O4-Mn3-N4	114.92(9)
Mn3−N31	2.567(4)	N2-Mn3-N4	100.6(1)
Mn3−O3	2.309(3)	Mn3-N2-C2	176.4(3)
Mn3−O4	2.190(3)	Mn3-N4-C4	158.1(3)
W1−C1	2.176(4)	C1-W1-C3	72.3(2)
W1−C2	2.159(4)	C2-W1-C4	72.8(2)
W1−C3	2.161(4)	W1-C1-N1	176.4(4)
W1−C4	2.177(4)	W1-C2-N2	178.2(4)
C1−N1	1.144(5)	W1-C3-N3	178.3(4)
C2−N2	1.149(5)	W1-C4-N4	177.8(4)
C3−N3	1.150(6)		
C4−N4	1.146(5)		
W2−C9	2.189(5)	C9-W2-C10	72.6(2)
W2−C10	2.130(7)	W2-C9-N9	176.7(4)
C9−N9	1.147(6)	W2-C10-N10	179.1(6)
C10−N10	1.139(8)		
7			
Mn1−N1	2.256(3)	N9-Mn1-N11	134.6(1)
Mn1−N2	2.166(3)	N9-Mn1-N10	66.5(1)
Mn1−N9	2.536(3)	N10-Mn1-N11	68.5(1)
Mn1−N10	2.322(3)	O1-Mn1-O2	86.2(1)
Mn1−N11	2.424(3)	N2-Mn1-O2	173.7(1)
Mn1−O1	2.299(3)	N1-Mn1-N2	91.4(1)
Mn1−O2	2.153(2)	Mn1-N1-C1	166.5(3)
		Mn1-N2-C2	159.8(3)
Mn2−N3	2.215(3)	N15-Mn2-N17	139.2(1)
Mn2−N15	2.370(3)	N15-Mn2-N16	69.7(1)
Mn2−N16	2.247(3)	N16-Mn2-N17	69.5(1)
Mn2−N17	2.392(3)	N3-Mn2-O6	178.3(1)
Mn2−O3	2.330(3)	N3-Mn2-O3	86.2(1)
Mn2−O4	2.284(3)	O3-Mn2-O6	94.2(1)
Mn2−O6	2.164(3)	Mn2-N3-C3	153.8(3)
W1−C1	2.164(3)	C1-W1-C2	73.5(1)
W1−C2	2.159(3)	C1-W1-C3	137.9(1)
W1−C3	2.165(3)	W1-C1-N1	178.2(3)
C1−N1	1.138(4)	W1-C2-N2	177.7(3)
C2−N2	1.138(4)	W1-C3-N3	175.9(3)
C3−N3	1.142(4)		
8			
Mn1−N1	2.167(4)	N17-Mn1-N19	141.6(1)
Mn1−N4	2.228(4)	N17-Mn1-N18	71.3(1)
Mn1−N17	2.329(4)	N18-Mn1-N19	70.4(1)
Mn1−N18	2.212(3)	O1-Mn1-N4	164.4(1)
Mn1−N19	2.341(4)	N1-Mn1-N4	92.0(2)
Mn1−O1	2.199(3)	Mn1-N1-C1	166.2(4)
		Mn1-N4-C4	153.9(3)
Mn2−N9	2.207(4)	N23-Mn2-N25	141.5(1)
Mn2−N14	2.169(4)	N23-Mn2-N24	70.9(1)
Mn2−N23	2.317(4)	N24-Mn2-N25	70.7(1)
Mn2−N24	2.190(4)	N9-Mn2-O2	166.2(1)
Mn2−N25	2.336(4)	N9-Mn2-N14	92.4(2)
Mn2−O2	2.204(4)	Mn2-N9-C9	154.9(4)
		Mn2-N14-C14	164.4(4)
Mn3−N11	2.139(4)	N29-Mn3-N31	142.0(1)
Mn3−N29	2.323(3)	N29-Mn3-N30	70.8(1)
Mn3−N30	2.191(3)	N30-Mn3-N31	71.28(9)
Mn3−N31	2.295(3)	O3-Mn3-O4A	171.4(1)
Mn3−O3	2.166(3)	O3-Mn3-N11	86.4(1)
Mn3−O4A	2.172(3)	Mn3-N11-C11	167.3(4)

Table 4. (Continued)

8			
W1−C1	2.161(4)	C1-W1-C4	138.9(2)
W1−C4	2.165(4)	W1-C1-N1	175.9(4)
C1−N1	1.164(5)	W1-C4-N4	173.6(4)
C4−N4	1.157(6)		
W2−C9	2.180(5)	C9-W2-C11	76.3(2)
W2−C11	2.158(4)	C9-W2-C14	138.7(2)
W2−C14	2.180(5)	W2-C9-N9	172.8(4)
C9−N9	1.150(6)	W2-C11-N11	178.0(4)
C11−N11	1.156(5)	W2-C14-N14	176.6(4)
C14−N14	1.148(6)		

The chains run parallel to the *c* axis and interact with each other through extensive π–π contacts between tptz ligands (Figure 3b). Such interdigitation of the neighboring chains results in layers (slabs) of chains parallel to the *ac* plane (Figure 3c). The interaction between the layers occurs through hydrogen bonding of the C≡N···HC type between the cyanide ligands of $[W(CN)_8]^{4-}$ fragments of one layer and pyridyl hydrogen atoms of the tptz molecules of the adjacent layer (Figure 3d).

Chains of squares have been observed previously in several cyanide-bridged bimetallic systems assembled from $[M(CN)_8]^{3-/4-}$ anions (M = Mo, W) and transition metal ions. In $[Cu^{II}(tetrenH_2)]_2[W^{IV}(CN)_8]_2\cdot 5H_2O$,[30] Cu_2W_2 square fragments are connected into a 1D structure through CN^- ligands which bridge W and Cu corners of adjacent squares. In $[Mn^{II}_3(bpy)_2(DMF)_8][M^V(CN)_8]_2$,[31,32] Mn_2M_2 squares are bridged into a chain by additional Mn ions which coordinate to the available CN^- ligands of the M sites. The compound $[Cu^{II}(tetrenH_2)][Cu^{II}(tetrenH)][W^V(CN)_8][W^{IV}(CN)_8]\cdot 2.5H_2O$[30] adopts a 1D ribbon structure assembled from edge-sharing Cu_2W_2 squares. In the structure of **4**, a chain of vertex-sharing squares is observed, which is an unprecedented structural motif in the chemistry of cyanide-bridged complexes based on $[M(CN)_8]^{3-/4-}$ anions.

$\{[Mn_2(tptz)_2(MeOH)_3(OAc)][W(CN)_8]\cdot 3.5MeOH\cdot 0.25H_2O\}_\infty$ (5): When the starting materials used to prepare complex **3** are reacted in anhydrous MeOH, compound **5** is formed. The asymmetric unit in the crystal structure of **5** contains two crystallographically unique Mn centers, both in heptacoordinate environments (Figure 4a). The coordination of Mn1 is similar to that observed for the Mn2 center in structure **3**. The environment consists of one tridentate tptz molecule and one chelating OAc^- anion in the equatorial plane of the pentagonal bipyramid, with the axial sites of the bipyramid being occupied by an MeOH molecule and a bridging CN^- ligand. The coordination environment of Mn2 consists of one tptz ligand, two MeOH molecules, and two bridging cyanides and can be described as a distorted monocapped trigonal prism. Two trigonal basal planes are formed by atoms N17, N16, O5 and O4, N5, N1, respectively, and the N15 atom caps the O5-N16-N5-N1 rectangular face. The central Mn2 atom is shifted toward this rectangular face in the direction of the N15 atom, although the Mn2–N15 distance (2.434(3) Å) is longer than the distances from Mn2 to the other six atoms (2.203(3)–2.415(3) Å) that form the trigonal prism. The W1 center is surrounded by three bridging and five terminal CN^- ligands in a square antiprismatic arrangement. Two of the bridging cyanides connect W1 and Mn2 centers into an infinite zigzag chain that propagates along the *c* axis (Figure 4b). The third bridging cyanide serves to connect the Mn1 atom to the side of the chain by linking it to the W1

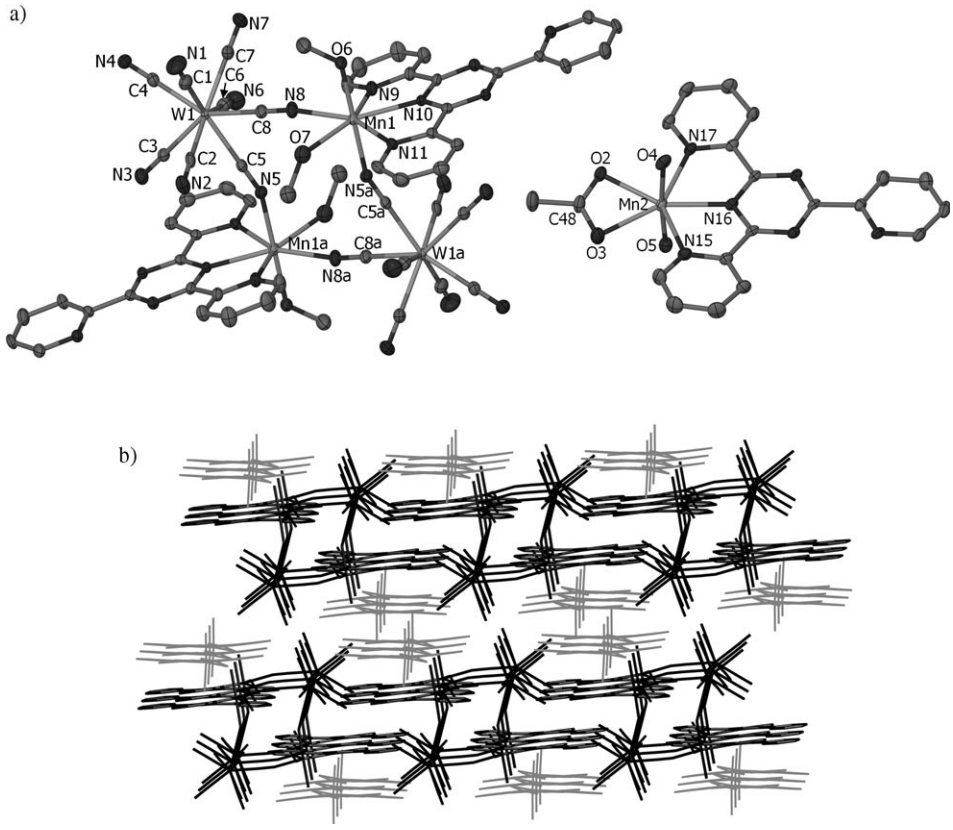

Figure 2. a) Depiction of the asymmetric unit in the crystal structure of **3** showing separately the anionic square (left) and the mononuclear cation (right) (thermal ellipsoids are drawn at the 50% probability level, and H atoms are omitted for the sake of clarity). b) View of the crystal structure packing in **3** approximately down the *c* axis, with the anionic squares emphasized with darker and thicker bonds.

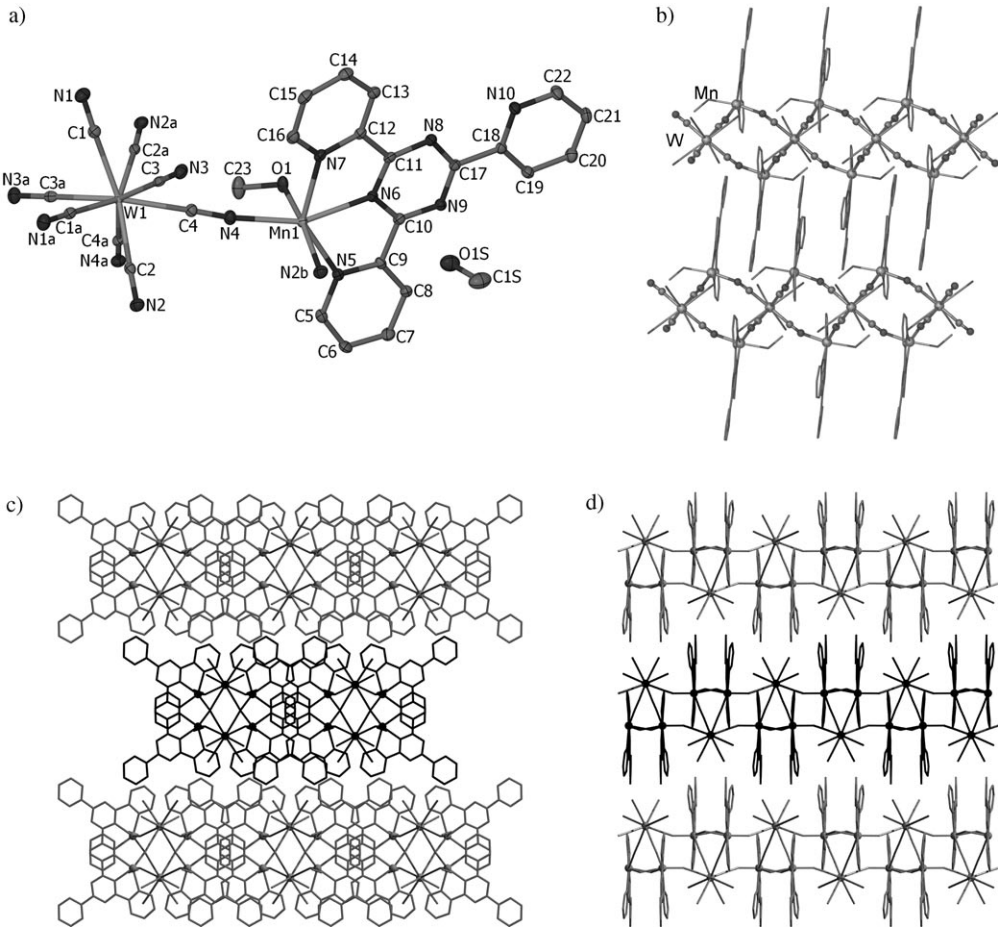

Figure 3. a) The asymmetric unit of **4** (thermal ellipsoid plot at the 50% probability level; H atoms are omitted for the sake of clarity). b) Two adjacent chains of squares depicting the interdigitated tptz ligands. The cyanide-bridged core is emphasized with thicker bonds. c) View of the crystal structure down the *c* axis, showing the layers of interdigitated chains. The alternating layers are highlighted with different shades of gray, and the metal sites are shown as spheres. d) View down the *a* axis. The $[W(CN)_8]^{4-}$ fragments of one layer interact with the tptz molecules of the neighboring layer (see text). (In b)–d), solvent molecules and H atoms are omitted for the sake of clarity.)

atom. A similar zigzag chain of cyanide-bridged Mn and Mo centers with pendant Mn arms was observed in the structure of $[Mn^{II}_2(L_5)_2(H_2O)][Mo^{IV}(CN)_8]\cdot 5H_2O$.[33]

The crystal packing in structure **5** is similar to that observed for **4**. The chains run along the *c* axis and interact with each other through extensive face-to-face π–π contacts (Figure 4b). These interactions lead to the formation of two-dimensional slabs in the *ac* plane. In contrast to **4**, in which the layers of π–π interacting chains are nearly flat (Figure 3d), in **5** the layers are buckled, with each chain exhibiting a buckled motif (Figure 4c). Solvent molecules occupy the spaces between the layers and engage in hydrogen bonding with the octacyanotungstate fragments.

The structure of **5**, as described above, is based on viewing it as a zigzag chain of cyanide-bridged Mn^{II} and W^{V} ions, with pendant Mn^{II} ions dangling from the chain. An alternative way to describe this structure is to view it as a chain of vertex-sharing squares, such as those present in structure **4** (Scheme 1), with one Mn-N≡C-W link in each of the squares being cleaved. In considering the reasons for the formation of the different structures, it is reasonable to suggest that the driving force for the formation of **4** and **5** is the neutrality of the resulting phase which facilitates their crystallization in the polar solvents used for the syntheses. The combination of one $[W(CN)_8]^{4-}$ anion with two Mn^{II} ions results in the crystallization of the neutral 1D compound **4** in the form of vertex-sharing squares. When the $[W(CN)_8]^{3-}$ anion is used, however, its combination with two Mn^{II} ions requires an extra negative charge to achieve neutrality. Therefore, the asymmetric unit of structure **5** contains one acetate ion that acts as a chelating ligand to the Mn1 center and prevents the latter from binding to CN^- ligands of the neighboring $[W(CN)_8]^{3-}$ moiety in the same fashion as in compound **4**.

$[Mn_6(tptz)_6(MeOH)_4(DMF)_2W_4(CN)_{32}]\cdot 8.2H_2O\cdot 2.3MeOH$ (6): The asymmetric unit in the crystal structure of **6** contains three Mn and two W atoms (Figure 5a). The Mn1, Mn2, W1, and W2 centers form a cyanide-bridged square, and two such squares are connected to each other via two Mn3 atoms. The resulting centrosymmetric decanuclear complex consists of three vertex-sharing cyanide-bridged

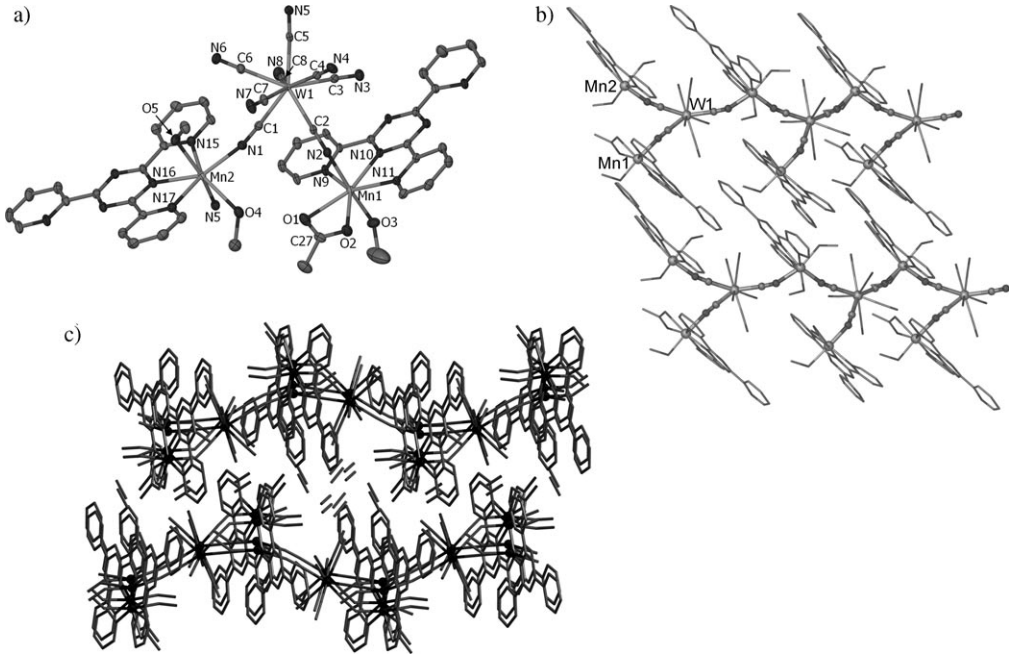

Figure 4. a) A depiction of the asymmetric unit of **5** (thermal ellipsoid plot at the 50% probability level; solvent molecules and H atoms are omitted for the sake of clarity). b) Two adjacent chains showing the interdigitated tptz ligands. The cyanide-bridged motif is accentuated with thicker bonds. c) View of the crystal structure approximately down the *a* axis, showing the buckled layers of interdigitated chains. Solvent molecules occupy the interlayer space. Mn and W sites are shown as black spheres.

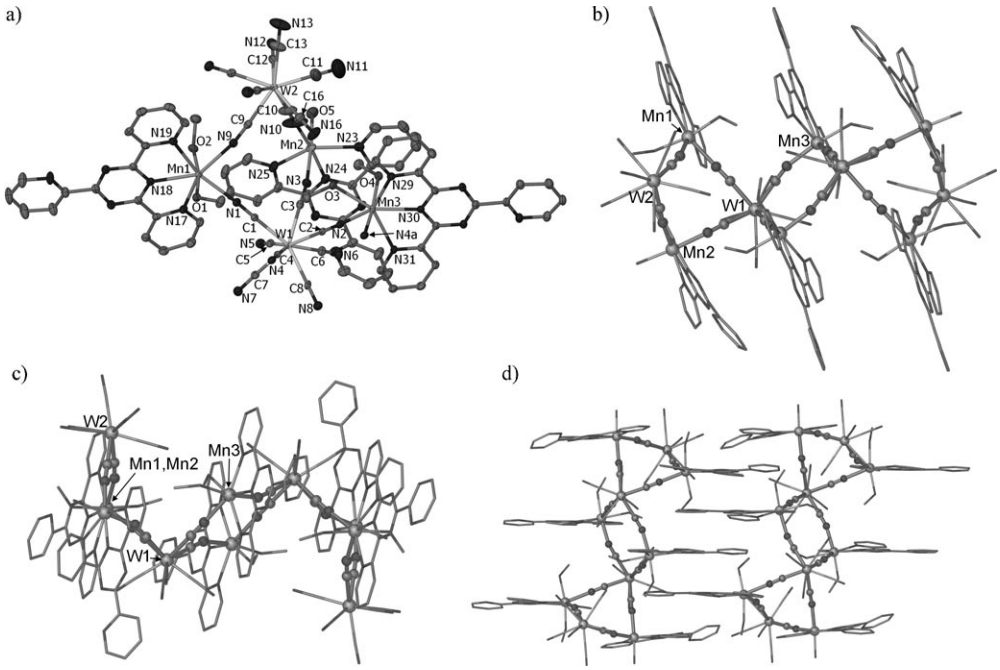

Figure 5. a) A depiction of the asymmetric unit of **6** (thermal ellipsoid plot at the 50% probability level; H atoms and solvent molecules are omitted for the sake of clarity). b), c) Two different views of the decanuclear cluster built of three vertex-sharing squares. The cyanide-bridged core of the cluster is emphasized with thicker bonds. d) A depiction of the π–π interactions between tptz ligands of two adjacent decanuclear clusters.

squares, with the shared vertices being the W1 atoms (Figure 5b).

The heptacoordinate Mn1 and Mn3 centers are in distorted pentagonal bipyramidal environments that consist of one tridentate tptz ligand, two N-bound bridging cyanides, and two MeOH molecules. In the case of Mn1, the equatorial plane of the bipyramid is formed by the N donor atoms of tptz and the CN^- ligands and the axial positions are occu-

pied by the O atoms of MeOH molecules. For Mn3, the equatorial plane of the pentagonal bipyramid includes three N atoms of the tptz ligand, one N atom of the bridging CN^-, and one O atom of the MeOH molecule. The remaining CN^- and MeOH ligands occupy the axial positions of the bipyramid. The Mn–N distances for Mn1 and Mn3 centers are in similar ranges (2.298(4)–2.511(4) and 2.190(4)–2.567(4) Å, respectively). The Mn3–N4 bond is somewhat shorter than the distances from Mn1 and Mn3 atoms to other CN^- ligands (Table 4). This can be easily understood taking into account that the N4 atom occupies the less crowded axial position of the pentagonal bipyramid. The same effect is observed in the Mn–O distances; the equatorial Mn3–O3 bond (2.309(3) Å) is notably longer than the axial Mn3–O4 bond (2.190(3) Å) or the axial Mn1–O bonds (2.179(3) and 2.199(3) Å).

In contrast to the Mn1 and Mn3 centers, the Mn2 atom is in a distorted octahedral environment composed of one tridentate tptz ligand, two N-bound bridging cyanides, and one water molecule. The distortion is mainly due to the bite angle of the tptz ligand ($\approx$142°). The decreased coordination number results in the shorter Mn2–N and Mn2–O5 bonds (2.103(6)–2.329(4) and 2.151(4) Å, respectively), as compared to the bond lengths observed for the Mn1 and Mn3 atoms. The W1 and W2 atoms are in an eight-coordinate environment of CN^- ligands. The W2 center belongs only to the peripheral square and, therefore, is surrounded by two bridging and six terminal cyanides in a square antiprismatic configuration. On the other hand, the W1 site is shared by the peripheral and central squares, and its coordination environment consists of four bridging and four terminal cyanide ligands. The geometry of the W1 ion is more distorted and, using the dihedral angle criterion defined by Porai–Koshits and Aslanov,[34] can be described as being intermediate between a square antiprism and a bicapped trigonal prism. (The criterion takes into account the degree of out-of-plane twist of two trapezoids defined by C1-C3-C6-C8 and C2-C4-C7-C5 vertices.) The distortion is similar to that observed for the $[W(CN)_8]^{3-}$ anion in the crystal structure of $Na_3[W(CN)_8]$.[35]

From the topological point of view, compound **6** can be considered to be a truncated version of **4** (Scheme 1). The view of the decanuclear cluster **6** in Figure 5c reveals that the peripheral squares are quite distorted and adopt a butterfly shape, while the overall shape of the cluster core resembles two boats fused together at the Mn3 centers. The tptz ligands are arranged on both sides of the cluster, roughly perpendicular to the direction of the truncated chain of squares. Such an arrangement provides sufficient space for intercalation of another aromatic system between two adjacent tptz ligands, which allows for efficient packing of decanuclear clusters dominated by interdigitation of the tptz ligands from neighboring molecules and extensive π–π stacking interactions (Figure 5d).

The formation of **6** can also be rationalized on the basis that it is a neutral structure. As mentioned earlier, the decanuclear cluster present in **6** can be viewed as being derived from an infinite chain of the vertex-sharing squares observed in **4** (Scheme 1). In the latter, the combination of two Mn^{II} ions and one $[W^{IV}(CN)_8]^{4-}$ ion results in an overall neutral charge for the chain of squares. If the same chain were to be formed with the $[W^{V}(CN)_8]^{3-}$ anion, the resulting structure would have a net positive charge (+1 per each square). The truncation of the chain observed in structure **6** results in a neutral cluster composed of three vertex-sharing squares. It also should be pointed out that the Mn2 sites are coordinated to H_2O molecules, while coordination environments of the Mn1 and Mn3 centers involve MeOH molecules. Given that the formation of **6** involves H_2O, the reaction was conducted in an anhydrous solvent which led to compound **7** that exhibits a completely different crystal structure.

$\{[Mn_2(tptz)_2(MeOH)_3W(CN)_8][Mn(tptz)(MeOH)W(CN)_8]\cdot 2H_2O\cdot MeOH\}_8$ (7): The crystal structure of **7** features two extended structural fragments, both of which are based on a zigzag chain of cyanide-bridged metal ions. The anionic chain is based on the combination of cyanide-bridged Mn1 and W1 sites, while the backbone of the cationic chain is composed of cyanide-bridged Mn2 and W2 centers, with a dangling Mn3 site being attached via cyanide ligand to each W2 center (Figure 6a).

All of the Mn sites in structure **7** exhibit a distorted octahedral coordination composed of a tridentate tptz ligand and three monodentate ligands (two bridging cyanides and one MeOH molecule for the Mn1 and Mn2 atoms and one bridging cyanide and two MeOH molecules for the Mn3 atom). As observed for other structures described in this work that contain both hepta- and hexacoordinate Mn^{II} ions (**3**, **5**, and **6**), the decrease in the coordination number results in shortening of Mn–N and Mn–O bond lengths. This trend is also observed in structure **7**, where the Mn to ligand distances are in the range of 2.139(4)–2.341(4) Å which compares well to the metric parameters of hexacoordinate Mn^{II} sites in the aforementioned structures. Both W1 and W2 centers are in square antiprismatic coordination environments composed of two bridging and six terminal CN^- ligands and three bridging and five terminal CN^- ligands, respectively.

Both cationic and anionic chains propagate along the *a* axis, with the interchain interactions taking place through face-to-face π–π contacts (Figure 6b). The π–π contacts are observed for the cation-cation and cation–anion arrangements but not for the anion–anion case (Figure 6c). Secondary interchain communications are mediated by solvent molecules which engage in hydrogen bonding with terminal CN^- ligands of the octacyanotungstate units.

The structure of the cationic fragment in **7** resembles that of the neutral chain in the crystal structure of **5**. The neutrality of the chain in **5** was ensured by the coordination of a chelating acetate anion to the dangling Mn site. In **7**, however, an additional anion is not coordinated to either of the Mn centers, which results in an overall positive charge for the chain composed of two Mn^{II} and one $[W^{V}(CN)_8]^{3-}$ ions

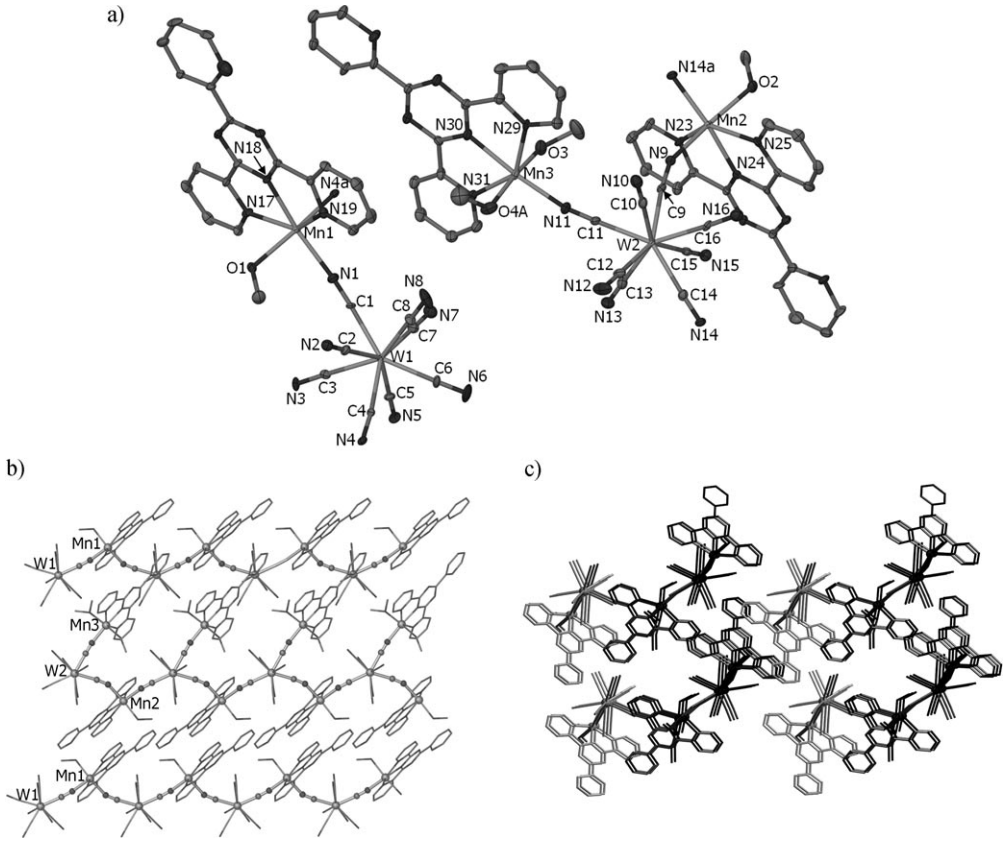

Figure 6. a) Depiction of the asymmetric unit of **7** (thermal ellipsoid plot at the 50% probability level; H atoms and solvent molecules are omitted for of clarity.). b) Drawings of adjacent chains emphasizing how the tptz ligands of the central cationic chain engage in face-to-face π–π contacts with the tptz ligands of adjacent anionic chains. The cyanide-bridged core is emphasized with thicker bonds. c) Packing of the chains viewed approximately down the *a* axis. The cationic chains are darker and the anionic chains are lighter.

and a negative charge for the chain composed of one Mn^{II} and one $[W(CN)_8]^{3-}$ ions. It is interesting to note that Cl^- does not participate in the formation of either **6** or **7**. Clearly, the co-crystallization of the complex cation and anion in **7** is preferable to the crystallization of the cation with a Cl^- counterion or to the formation of a neutral structure in which a Cl^- anion is coordinated to one of Mn centers. The cationic and anionic sub-lattices in **7** engage in extensive π–π stacking interactions which favor the formation of the double chain motif.

$[Mn(tptz)(MeOH)(NO_3)]_2[Mn(tptz)(MeOH)(DMF)]_2[W(CN)_8]_2\cdot 6MeOH$ (8): The crystal structure of **8** consists of a hexanuclear cluster based on an $Mn^{II}{}_2W^{V}{}_2$ square fragment with two dangling Mn^{II} ions (Scheme 1). The square is formed by cyanide-bridged Mn1 and W1 sites (Figure 7a), with the two halves of the square being related by an inversion center. The dangling Mn2 atoms are connected via cyanide bridges to the W1 corners of the square. Both Mn1 and Mn2 sites are in a pentagonal bipyramidal coordination environment. The Mn1 center is surrounded in the equatorial plane by a tridentate tptz ligand, one bridging cyanide, and one DMF molecule, while the axial positions are occupied by another bridging cyanide and an MeOH molecule. The Mn2 ion is coordinated to a tridentate tptz molecule and a bidentate NO_3^- anion in the equatorial plane and a bridging CN^- ligand and an MeOH molecule in the axial positions, which is very similar to the coordination of the Mn center observed in the mononuclear complex **2**; the ranges of the equatorial and axial bond lengths are similar in both cases (2.247(3)–2.392(3) and 2.164(3)–2.215(3) Å, respectively, in **8**; and 2.230(3)–2.370(3) and 2.154(3)–2.192(3) Å, respectively, in **2**). The W1 ion is in a square antiprismatic coordination environment of three bridging and five terminal CN^- ligands. Although the N1-Mn1-N2 angle (91.4(1)°) is nearly ideal for the formation of a molecular square, the C1-W1-C2 angle of 73.5(1)° is much more acute which leads to the distortion of the square into a shape more similar to that of a rhombus. The distortion is also reflected in the deviation of Mn1-N1-C1 and Mn1-N2-C2 angles from linearity (166.5(3) and 159.8(3)°, respectively).

The principal interaction between the hexanuclear units takes place via face-to-face π–π stacking of the tptz ligands (Figure 7b). Each cluster forms two such π–π contacts on one side of the square and two on the other side, with the tptz molecule coordinated to the Mn1 center being engaged in interactions with the tptz molecule at the Mn2 site of the neighboring cluster. Such an arrangement leads to efficiently

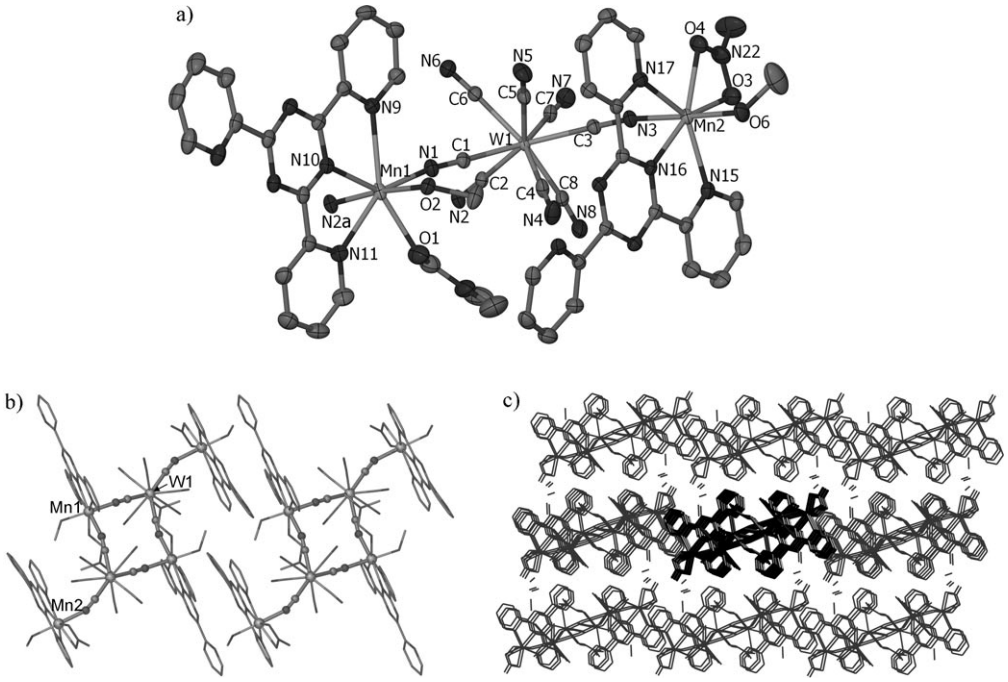

Figure 7. a) A depiction of the asymmetric unit of **8** (thermal ellipsoid plot at the 50% probability level; H atoms and solvent molecules are omitted for the sake of clarity). b) π–π interactions between two adjacent hexanuclear clusters resulting in stacking of clusters along the *a* axis (horizontal direction). The cyanide-bridged cores of the clusters are highlighted by thicker bonds. c) View approximately down the *a* axis, depicting π–π interactions between the neighboring stacks of clusters. The central stack is shown with thicker bonds.

packed stacks of clusters parallel to the *a* direction of the unit cell (Figure 7c). Interactions between the adjacent stacks also occurs through π–π contacts which are not as strong as those observed within each stack. These secondary π–π interactions lead to the formation of two-dimensional slabs parallel to the *ac* plane. The space between the slabs is occupied by solvent molecules which are hydrogen bonded to the nitrate anions coordinated to the Mn2 centers.

The crystallization of **8** appears to be driven by the neutrality of the resulting hexanuclear complex, the trend which was observed for all but compound **7** in this study. Cluster **8** is unique in the chemistry of heteronuclear complexes based on $[M(CN)_8]^{3-/4-}$ anions (M = Mo, W), although a topologically similar fragment was described by Kim et al. in a series of complexes $\{[(Tp)Fe(CN)_3]_4[M(MeCN)(H_2O)_2]_2]\}\cdot 10H_2O\cdot 2MeCN$ (M = Mn, Co, Ni).[36] In these compounds, two $[(Tp)Fe(CN)_3]$ fragments are attached via bridging cyanides to a central Fe_2M_2 square unit.

Remarks regarding the structures of compounds 3–8: A few generalizations can be made from an analysis of the crystal structures presented in this study. The structural flexibility of the octacyanotungstate anion allows for the formation of diverse cyanide-bridged structural motifs with only subtle changes in the synthetic conditions. Although the resulting structure depends on a variety of factors, including the choice of counterion, the extent of π–π interactions and hydrogen bonding, and the ratio of metal ions introduced into the reaction, except for compound **7**, the products crystallize as neutral species (chains or multinuclear complexes), with the crystallization of such species being driven by the use of polar solvents as a reaction medium. Another pertinent observation is that the preferred coordination of the Mn^{II} ions is heptacoordinate which stems from the bite angle defined by the pyridyl nitrogen atoms of the tptz ligand, the average value of this angle being 138°. This angle imposes a coordination geometry close to an ideal pentagonal bipyramid, in which the ideal angle is 144°. Indeed, in most of the structures described above, the Mn^{II} ion is in a pentagonal bipyramidal environment, and the trischelating tptz ligand provides three of the five donor atoms for the equatorial plane of the bipyramid. Finally, a square unit composed of cyanide bridged Mn and W ions appears to be a ubiquitous structural fragment in these compounds. As has been seen, even structures **5** and **7**, which formally do not contain such square units, can be described as being derived from structure **4** based on vertex-sharing squares (Scheme 1). As will be described in the following section, such structural similarities have ramifications on the magnetic behavior of these compounds.

Magnetic properties

Compound 3: DC magnetic susceptibility measurements revealed that the χT value of **3** gradually decreases from 17.3 emu mol^{-1} K at 300 K to a broad minimum at about 50 K, then increases to a maximum value of 17.5 emu mol^{-1} K at 8.0 K, and finally decreases at lower temperatures (Figure 8). The value observed at room temperature is slightly lower than the theoretically expected χT

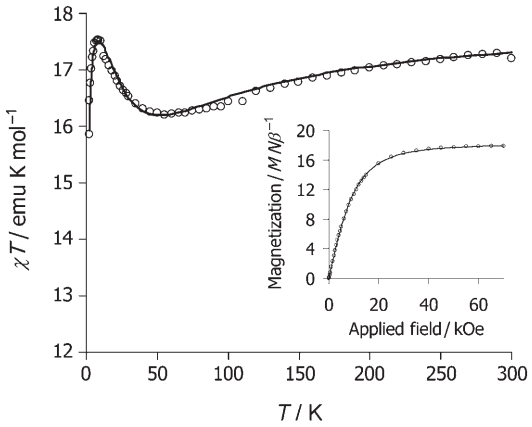

Figure 8. Temperature dependence of the χT product for **3** (○). The solid line corresponds to the MAGPACK simulation, including the mean-field approximation to account for intermolecular coupling at lower temperatures ($g_{Mn}=1.99$, $g_W=2.00$, $J=-7.8\ cm^{-1}$, $zJ'=-0.03\ cm^{-1}$; $R2=0.9994$). Inset: Field dependent magnetization (○). The solid line correspond to the best fit to the Brillouin function (see text; $R2=0.9988$). [The correlation value is defined as $R2=1-\sqrt{\frac{\sum(\chi T_{obs}-\chi T_{calcd})^2}{(n-p)\times\sum(\chi T_{obs})^2}}$, where n is the number of experimental data points and p is the number of refined parameters.]

value for magnetically non-interacting four Mn^{II} ($S_{Mn}=5/2$) and two W^V ($S_W=1/2$) ions. This fact, along with the temperature behavior of the χT curve, suggests that antiferromagnetic interactions are occurring between the Mn^{II} and W^V centers. These interactions are mediated by the CN^- ligands of the square fragment (see Figure 2) and can be described using the following Hamiltonian:

$$H=-2J\cdot(S_{W1}+S_{W1a})\cdot(S_{Mn1}+S_{Mn1a}) \quad (1)$$

where J is an isotropic magnetic exchange constant. The temperature dependence of χT was simulated with MAGPACK,[37] taking into account the contribution from two non-interacting Mn^{II} centers that belong to the cationic units. The decrease of χT at temperatures below 8.0 K can be attributed to weak intermolecular coupling which is, probably, mediated by hydrogen bonding and π–π stacking interactions. The mean-field approximation was used to account for this effect. The fitting of the χT curve resulted in the final parameters $g_{Mn}=1.99$, $g_W=2.00$, $J=-7.8\ cm^{-1}$, and $zJ'=-0.03\ cm^{-1}$. The value of the magnetic exchange constant J is comparable to the value of $-6.0\ cm^{-1}$ reported for the pentanuclear V-shaped cluster $[Mn^{II}_3(bpy)_6(H_2O)][W^V(CN)_8]_2$.[38]

The antiferromagnetic coupling between Mn^{II} and W^V ions in the square fragment leads to the stabilization of a high spin ground state, which results in the maximum in the χT vs. T dependence at lower temperatures. Magnetization measurements performed in a variable applied magnetic field at 1.8 K (Figure 8, inset) confirmed the assignment of the antiferromagnetic ground state for the square fragment ($S=4$ and $g=2.00$), after taking into account the presence of two non-interacting Mn^{II} centers with $S=5/2$ and $g=2.00$.

Compound 4: Compound **4** exhibits a room temperature χT value of 8.83 emu mol^{-1} K, which is close to the theoretically expected spin-only value of 8.75 emu mol^{-1} K for two non-interacting Mn^{II} centers with $S=5/2$ (see Supporting Information, Figure S1). The χT product remains nearly constant over the entire studied temperature interval. The decrease in χT below 10 K is attributed to intermolecular magnetic interactions between neighboring paramagnetic chains of squares (Figure 3). The temperature dependence of the magnetic susceptibility was fitted to the Curie–Weiss law, with a negative Weiss constant $\theta=-0.7$ K in accord with weak antiferromagnetic interchain interactions.

Compound 5: The χT value of **5** at 300 K is 9.30 emu mol^{-1} K, which is close to the spin-only value of 9.13 emu mol^{-1} K expected for two non-interacting Mn^{II} and one W^V centers. The value decreases slowly to a minimum of 9.00 emu mol^{-1} K at 95 K and then increases to a sharp maximum and reaches the highest value of 28.1 emu mol^{-1} K at 3.5 K (Figure 9). Such behavior is typical for a ferrimagnetic chain with alternating metal centers of a different spin state.[39,40] Compound $[Mn^{II}_2(L_5)_2(H_2O)][Mo^{IV}(CN)_8]\cdot 5H_2O$[33] is structurally similar to **5** and exhibits very similar magnetic properties after being irradiated with UV light. The irradiation leads to photooxidation of Mo^{IV} to Mo^V and formation of spin centers of the values observed in **5**. Interestingly, the minimum of χT in this earlier reported compound is also observed at 95 K.

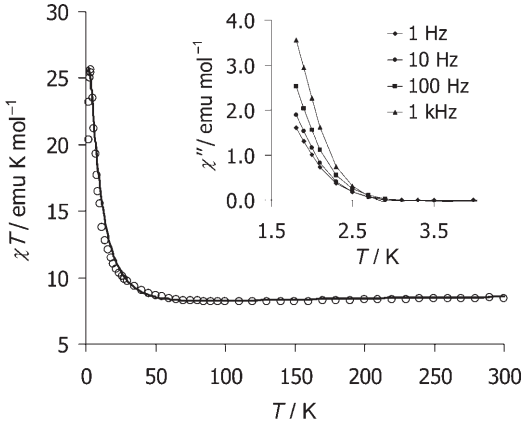

Figure 9. Temperature dependence of the χT product for **5** (○). The solid line corresponds to the MAGPACK simulation ($g_{Mn}=g_W=1.97$, $J=-6.1\ cm^{-1}$, $zJ'=-0.005\ cm^{-1}$; $R2=0.9893$). Inset: Temperature dependence of the imaginary component χ'' of the AC magnetic susceptibility at different frequencies under applied magnetic field $H_{AC}=3$ Oe and $H_{DC}=0$ Oe. (Solid lines are guides for eye.)

The sharp maximum in the χT dependence suggests the onset of magnetic ordering below 3.5 K, which occurs due to interchain interactions. This conclusion is also supported by the appearance of an out-of-phase signal in the AC magnetic susceptibility measurement (Figure 9, inset). The field dependent magnetization measured in the range of 0–7 T at

1.8 K does not saturate and approaches a value of 9 μ_B (Figure S2, Supporting Information) expected for two Mn^{II} and one W^{V} ions, assuming antiferromagnetic coupling across the CN^- bridge.

Although several theoretical models have been developed for treating a ferrimagnetic alternating spin chain,[40,41] no model yet exists for such a chain with pendant arms, which precludes rigorous theoretical treatment of magnetic behavior of **5**. Nevertheless, the observed similarity in the magnetic behavior of **5** and **6** (see below) suggests that the value of the magnetic exchange constant in the former can be roughly estimated by approximating the chain by a truncated structure similar to the latter. Such a topology, depicted in Scheme 2 with a dashed rectangle and including 6 Mn^{II} and 3 W^{V} ions, can be treated with an isotropic Hamiltonian:

$$H = -2J \cdot [S_{W1} \cdot (S_{Mn1} + S_{Mn2}) + S_{W1a} \cdot (S_{Mn2} + S_{Mn1a} + S_{Mn2a}) + S_{W1b} \cdot (S_{Mn2a} + S_{Mn1b} + S_{Mn2b})] \quad (2)$$

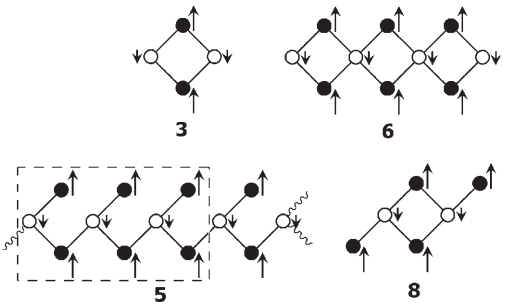

Scheme 2. Schematic representation of the antiferromagnetic spin coupling patterns in compounds **3**, **5**, **6**, and **8**. ●: Mn, ○: W.

where the isotropic exchange constant J is assumed to be equal for all pairs of interacting Mn^{II} and W^{V} ions, and symbols "a" and "b" indicate crystallographically equivalent atoms. To account for the intermolecular coupling at low temperatures, the resulting χT values were corrected using the mean-field theory. The simulation performed with MAGPACK[37] resulted in the values of $g_{Mn} = g_W = 1.97$, $J = -6.1\ cm^{-1}$, and $zJ' = -0.005\ cm^{-1}$, which are comparable to the values obtained for compounds **6** (see below) and give a reasonably good fit to the experimental data (Figure 9), thus confirming the validity of the suggested approximation. Nevertheless, it has to be emphasized that this approximation is very rough and might lead to underestimation of the zJ' parameter that characterizes the strength of intermolecular coupling.

Compound 6: For compound **6**, the room temperature χT value is 27.7 emu mol^{-1} K, which corresponds to the theoretically expected spin-only value for non-interacting six Mn^{II} and four W^{V} centers. The χT gradually decreases to a broad minimum of $\approx$27 emu mol^{-1} K around 100 K (Figure 10). Below this temperature, the χT product increases to a sharp maximum of 88.7 emu mol^{-1} K at 2.5 K, which is indicative of stabilization of a high spin ground state. Assuming antiferromagnetic coupling between Mn^{II} and W^{V} ions, the expected ground state spin value should be S = 13. This value is confirmed by the fitting of the field dependent magnetization to the Brillouin function for S = 13, g = 2.01 (Figure 10, inset).

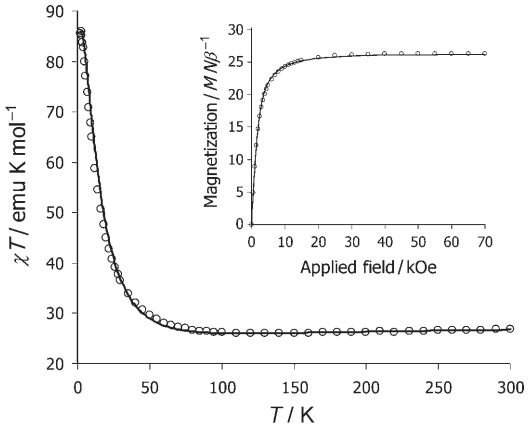

Figure 10. Temperature dependence of the χT product for **6** (○). The solid line corresponds to the MAGPACK simulation ($g_{Mn} = g_W = 2.01$, $J = -6.2\ cm^{-1}$, $zJ' = -7 \times 10^{-4}\ cm^{-1}$; $R2 = 0.9957$). Inset: Field dependent magnetization (○). The solid line correspond to the best fit to the Brillouin function (S = 13, $g = 2.01$; $R2 = 0.9982$).

To estimate the magnitude of magnetic coupling between Mn^{II} and W^{V} centers, the temperature dependence of χT was modeled with MAGPACK[37] using the isotropic Heisenberg–Dirac–Van Vleck Hamiltonian:

$$H = -2J \cdot [S_{W1} \cdot (S_{Mn1} + S_{Mn2} + S_{Mn3} + S_{Mn3a}) + S_{W2} \cdot (S_{Mn1} + S_{Mn2}) + S_{W1a} \cdot (S_{Mn1a} + S_{Mn2a} + S_{Mn3a} + S_{Mn3}) + S_{W2a} \cdot (S_{Mn1a} + S_{Mn2a})] \quad (3)$$

where J is the isotropic magnetic exchange constant, and Mn1/Mn1a, Mn2/Mn2a, Mn3/Mn3a, W1/W1a, and W2/W2a indicate crystallographically equivalent Mn and W centers in the decanuclear complex **6**. Due to the large size of the resulting energy matrix, and in order to avoid overparametrization, the exchange constant was assumed to be the same for all Mn^{II}-N≡C-W^{V} pairs of ions. The mean-field correction was applied to account for intermolecular magnetic interactions at low temperatures. The MAGPACK simulation resulted in the best-fit parameters $g_{Mn} = g_W = 2.01$, $J = -6.2\ cm^{-1}$, and $zJ' = -7 \times 10^{-4}\ cm^{-1}$.

It had already been noted in an earlier section that there is a structural relationship between complexes **5** and **6**. Both can be considered as being derived from structure **4**, the former being obtained by breaking one of the W-C≡N-Mn linkages in each square unit of **4** and the latter being a truncated variant of the chain of squares present in **4**. It should also be pointed out that compounds **5** and **6** are similar with regards to the spin topology of antiferromagnetic coupling across the W-C≡N-Mn bridge (Scheme 2). Although one of the cyanide links in each square fragment is missing in going

from **4** to **5**, the remaining bridging CN^- ligands ensure the same arrangement of spins as would be expected in the chain of vertex-sharing squares. Due to the similarity of their spin structure, compounds **5** and **6** exhibit a similar temperature dependence of their magnetic susceptibility (Figures 9 and 10). Clearly, even three ferrimagnetic squares linked into a short chain (**6**) are sufficient to exhibit magnetic behavior similar to an infinite ferrimagnetic chain (**5**). In contrast, molecular square **3** is characterized by a markedly different χT versus T curve, because of the smaller ground state spin value.

The decanuclear cluster present in the crystal structure of **6** is of considerable interest from the point of view of molecular magnetism, since it is the second largest cyanide-based molecular complex derived from the $[M^V(CN)_8]^{3-}$ anions (M = Mo, W), after the pentadecanuclear clusters $\{M'[M'^{II}(ROH)_3]_8[M^V(CN)_8]_6\}$ (M′ = Mn, Co, Ni; R = Me, Et).[13,22–25] The latter compounds behave as single-molecule magnets (SMMs), due to high ground state spin values and magnetic anisotropy. The high nuclearity of complex **6** and, consequently, its high ground state spin value render this molecule a promising scaffold for the development of new SMMs. Our future efforts in this vein will be directed at the modification of the tptz ligand to include bulkier peripheral substituents (for example, *tert*-butyl group), which will ensure better separation of the clusters and weaker intermolecular coupling. Results of these studies will be presented in due course.

Compound 7: The χT value of **7** at 300 K is 14.2 emu mol^{-1} K, which is only slightly higher than the spin-only value of 13.9 emu mol^{-1} K expected for three Mn^{II} and two W^V centers in the absence of magnetic coupling. The χT slightly decreases as the temperature is lowered and exhibits a broad minimum at $\approx$13.4 emu mol^{-1} K around 100 K. Below 50 K, the χT quickly increases to a sharp maximum of 102 emu mol^{-1} K at 3.5 K (Figure S3, Supporting Information). Such behavior is typical of a ferrimagnetic chain, while the decrease in χT at $T < 3.5$ K indicates an onset of bulk antiferromagnetic ordering due to interchain magnetic interactions. The existence of the ordered phase at lower temperatures is also supported by the AC magnetic susceptibility measurement which reveals an out-of-phase signal below 2.5 K (Figure S4, Supporting Information).

The expected magnetization saturation value should take into account the presence of two different ferrimagnetic chains in the crystal structure of **7** (Figure 6b and Scheme 1). The cationic chain is analogous to the structural fragment observed in **5** and contains two Mn^{II} ($S = {}^5/_2$ each) and one W^V ($S = {}^1/_2$) ions per formula unit. The anionic chain is a simple zigzag chain that consists of one Mn^{II} and one W^V center per formula unit. Based on the antiferromagnetic interactions between Mn^{II} and W^V ions via cyanide bridge, the expected magnetization saturation value is 13.0 μ_B for the spin-only case, which is only slightly smaller than the observed value of 13.5 μ_B (Figure S3, inset, Supporting Information).

The magnetic properties of **7** resemble the properties of compound **5**, which is the reflection of the similarity of ferrimagnetic chains present in their structures and, therefore, analogous spin coupling topology (Scheme 2) in the 1D structure of **5** and in the 1D cationic unit of **7**. Both compounds exhibit interchain magnetic interactions of a similar strength, judging by the onset of magnetic ordering that takes place at nearly the same temperature in both cases.

Compound 8: The 300 K χT value of **8** is 17.7 emu mol^{-1} K, only slightly lower than 18.3 emu mol^{-1} K expected for non-interacting four Mn^{II} and two W^V ions. The χT product slowly decreases to a minimum of 17.2 emu mol^{-1} K at 95 K, and then increases below 50 K reaching a maximum value of 47.2 emu mol^{-1} K at 2.0 K (Figure 11). Such behavior is indicative of antiferromagnetic coupling between Mn^{II} and W^V centers, with stabilization of a high spin ground state at low temperatures. The expected ground state of S = 9 was confirmed by fitting the field dependent magnetization curve to the Brillouin function assuming $g = 2.00$ (Figure 11, inset).

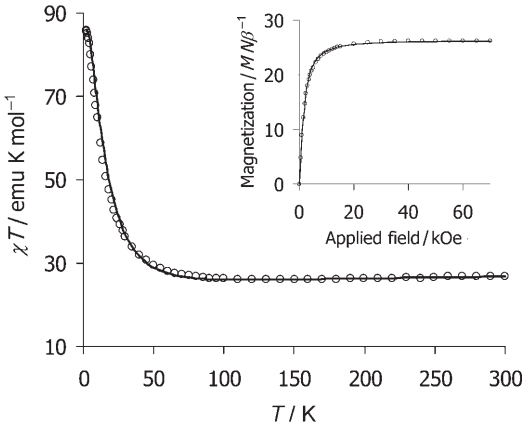

Figure 11. Temperature dependence of the χT product for **8** (○). The solid line corresponds to the MAGPACK simulation ($g_{Mn} = g_W = 2.01$, $J = -6.1$ cm^{-1}; $R2 = 0.9950$). Inset: Field dependent magnetization (○). The solid line correspond to the best fit to the Brillouin function (S = 9, $g = 2.00$; $R2 = 0.9971$).

The temperature dependence of χT was modeled with the isotropic Hamiltonian:

$$H = -2J \cdot [S_{W1} \cdot (S_{Mn1} + S_{Mn1a} + S_{Mn2}) + S_{W1a} \cdot (S_{Mn1} + S_{Mn1a} + S_{Mn2a})] \quad (4)$$

where J is an isotropic magnetic exchange constant, and Mn1/Mn1a, Mn2/Mn2a, and W1/W1a refer to crystallographically equivalent Mn and W centers in the hexanuclear complex **8**. Although the interaction of W^V ions with Mn^{II} ions within the square unit should be, strictly speaking, different as compared to the interaction of W^V with the pendant Mn^{II} ions (Figure 7), an approximation was used in which the same value of the magnetic exchange constant J was used for both interactions. Given the similar magnitude

of these coupling constants, such an approach avoids overparametrization during the fitting procedure. Simulation of the χT versus T curve with MAGPACK[37] resulted in $J = -6.1\ cm^{-1}$ and $g_{Mn} = g_W = 2.01$ (Figure 11).

To probe the possible SMM behavior of **8**, the temperature dependence of the AC magnetic susceptibility was measured at various frequencies (ν) of the applied magnetic field ($H_{AC} = 3$ Oe). The measurement performed in a zero static magnetic field ($H_{DC} = 0$) revealed normal paramagnetic behavior of the in-phase component χ' and absence of an out-of-phase signal χ'' (Figure S5, Supporting Information), thus showing that **8** does not behave as an SMM above 1.8 K (the lowest temperature of the experiment). Nevertheless, under a DC bias field, frequency dependent peaks appear in both χ' and χ'' (Figure 12). As the DC field is increased, the maximum of the out-of-phase signal is shifted to progressively higher temperatures. The relaxation rate $1/\tau = 2\pi\nu$ is temperature dependent and can be fitted to the Arrhenius law $\tau = \tau_0 \cdot \exp(U/k_B T)$, resulting in parameters $\tau_0 = 2.5 \times 10^{-6}$ s, $U = 6.1\ cm^{-1}$ at $H_{DC} = 1000$ Oe; $\tau_0 = 2.2 \times 10^{-7}$ s, $U = 12.9\ cm^{-1}$ at $H_{DC} = 2000$ Oe; $\tau_0 = 5.1 \times 10^{-8}$ s, $U = 16.2\ cm^{-1}$ at $H_{DC} = 3000$ Oe. Extrapolation of these results to $H_{DC} = 0$ gives $U_{H=0} = 1.6\ cm^{-1}$. The observed behavior suggests that the zero-field relaxation of magnetization in hexanuclear cluster **8** occurs too fast, which might be due to fast tunneling that is facilitated by transverse anisotropy terms and/or intermolecular interactions.[42] Application of the DC bias field leads to the suppression of resonant tunneling due to the mismatch of magnetic sublevels and increases the activation barrier U for the thermally activated relaxation.[43] These results hint at the potential of a molecule of this type to behave as an SMM. Our further efforts in this vein will be directed at modifying the blocking ligand in order to achieve better separation between the molecules thereby decreasing intermolecular interactions.

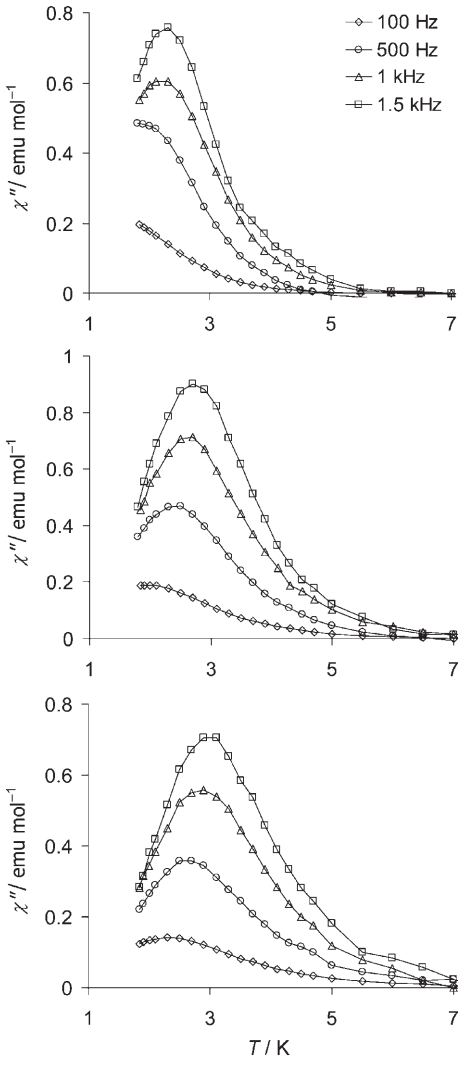

Figure 12. Imaginary part (χ'') of AC magnetic susceptibility of **8** measured in an applied magnetic field $H_{AC} = 3$ Oe under direct bias field H_{DC} of 1000 Oe (top), 2000 Oe (middle), and 3000 Oe (bottom).

Conclusions

A tridentate planar ligand capable of binding to a transition metal center in a *mer* fashion has not been explored prior to this study as a blocking ligand in the chemistry of cyanide complexes based on octacyanometalate anions. The present work makes use of the tridentate tptz ligand and, therefore, provides the first examples of compounds formed with a ligand of this type in such context. Analyses of the crystal structures reveal the ubiquity of the cyanide-bridged Mn_2W_2 square unit as a basic structural fragment for the bimetallic products. With this unit as a building block, various structural motifs are formed, beginning with the discrete molecular square **3**, to the decanuclear cluster **6** composed of three vertex-sharing squares to the infinite chain of vertex-sharing squares in **4**. The latter can also be considered as a parent structure from which the zigzag chains with pendant arms observed in structures **5** and **7** are derived.

The close relationships in the structures of the products also result in a similar topology for the magnetic interactions. For the bimetallic complexes **3** and **5**–**8**, antiferromagnetic coupling between Mn^{II} and W^{V} ions is propagated by the bridging CN^- ligands, resulting in ferrimagnetic ground states. The planarity of the square fragment may result in a higher magnetic anisotropy due to the mutual enhancement of single-ion anisotropies and, together with a high ground state spin value, could lead to observation of single-molecule and single-chain magnetism. In this regard, decanuclear complex **6** with ground state $S = 13$ was of special interest. We were unable, however, to observe a signature of SMM behavior in this compound in the absence of an applied DC field. Most likely, the different arrangement of three square units in its structure (Figure 5c) leads to the cancellation of single-ion anisotropies. Our future work will pursue the combination of $[M(CN)_8]^{3-}$ ions (M = Mo, W) with mononuclear tptz complexes of other transition metal ions with higher single-ion anisotropies, including Co^{II}, Mn^{III}, and V^{III} magnetic centers. We also plan to investigate the use of other tridentate meridional ligands with bulkier substituents

which should allow for better separation between the molecules or chains in the crystal structures, a requisite condition for the SMM or SCM behavior.

An interesting future direction for this work is the possibility for photoinduced magnetic behavior for complex **4**. Photooxidation of diamagnetic W^{IV} ions to paramagnetic W^{V} ions under irradiation with UV light should switch on the magnetic coupling between W and Mn centers and result in a dramatic increase of the magnetic moment due to the transition from a paramagnetic to a ferrimagnetic chain.[39] We are currently investigating the possibility of such a conversion and will report the results of our studies in due course.

Experimental Section

Starting materials: The reagents 2,4,6-tris(2-pyridyl)-1,3,5-triazine (tptz, Aldirch), $MnCl_2$ (Strem), $Mn(NO_3)_2{\cdot}4H_2O$, $Mn(OAc)_2{\cdot}4H_2O$ (Fisher) were used as received. The compound $[\{(C_4H_9)_3NH\}_3W(CN)_8]$ was prepared following the literature procedure.[44] All bimetallic complexes were prepared in reagent grade methanol (MeOH) and dimethylformamide (DMF), except for complexes **5** and **7** which were synthesized in additionally dried and distilled solvents.

$[Mn(tppz)(MeOH)Cl_2]{\cdot}H_2O$ (1): A solution of tptz (187 mg, 0.60 mmol) in MeOH (15 mL) was added dropwise to a solution of $MnCl_2$ (76 mg, 0.60 mmol) in MeOH (15 mL) with constant stirring. A yellow precipitate was observed to form gradually. The mixture was stirred for 30 min and then left undisturbed for 12 h. The resulting yellow solid was recovered by filtration, washed with MeOH (10 mL), and dried in air (245 mg, 84%). Single crystals of **1** were grown by slow diffusion of diethyl ether into a solution of **1** (20 mg) in MeOH/H_2O 4:1 (10 mL). Elemental analysis (%) calcd for **1** ($MnCl_2O_2N_6C_{19}H_{18}$): C 46.74, H, 3.72, N 17.21; found: C 46.51, H 3.20, N 18.07.

$[Mn(tptz)(NO_3)(H_2O)_2](NO_3){\cdot}1.5H_2O$ (2): A solution of tptz (187 mg, 0.60 mmol) in MeOH (15 mL) was added dropwise to a solution of $Mn(NO_3)_2{\cdot}4H_2O$ (151 mg, 0.60 mmol) in MeOH/H_2O 4:1 (15 mL) with stirring. A yellow solution formed instantaneously, and after a few minutes of stirring, a yellow precipitate formed. The mixture was stirred for 30 minutes and left to stand without stirring for 12 h. The yellow precipitate was harvested by filtration, washed with MeOH (10 mL), and dried in air (206 mg, 64%). Single crystals of **2** were grown by slow diffusion of diethyl ether into a solution of 20 mg of **1** in MeOH/water 4:1 (10 mL). Elemental analysis indicated that the interstitial solvent was partially lost when the sample was dried: elemental analysis calcd (%) for $[Mn(tptz)(NO_3)(H_2O)_2](NO_3){\cdot}0.5H_2O$ ($MnO_{8.5}N_8C_{18}H_{17}$): C 40.31, H 3.19, N 20.89; found: C 40.65, H 3.13, N 21.12.

$[Mn(tptz)(OAc)(H_2O)_2]_2\{[Mn(tptz)(MeOH)_{1.58}(H_2O)_{0.42}]_2[W(CN)_8]_2\}{\cdot}5MeOH{\cdot}9.85H_2O$ (3): A solution of tptz (125 mg, 0.40 mmol) in MeOH (8 mL) was slowly added to a solution of $Mn(OAc)_2{\cdot}4H_2O$ (98 mg, 0.40 mmol) in MeOH/H_2O 4:1 (10 mL) with stirring. The resulting dark yellow solution was layered in the dark with a solution of $[(C_4H_9)_3NH]_3W(CN)_8$ (190 mg, 0.20 mmol) in MeOH (10 mL). Large brown crystals were obtained after two weeks. The crystals were collected by filtration, washed with MeOH, and dried in vacuo (88 mg, 34%). Elemental analysis indicated that the interstitial solvent was lost when the sample was dried: elemental analysis calcd (%) for $[Mn(tptz)(OAc)(H_2O)_2]_2\{[Mn(tptz)(MeOH)_{1.58}(H_2O)_{0.42}]_2[W(CN)_8]_2\}$ ($W_2Mn_4O_{12}N_{40}C_{95.16}H_{76.32}$): C 44.65, H 3.01, N 21.89; found: C 43.62, H 2.77, N 21.96. IR (Nujol): $\tilde{\nu}$ = 2142, 2156, 2177 cm^{-1} (C≡N).

$\{[Mn^{II}(tptz)(MeOH)]_2[W^{IV}(CN)_8]{\cdot}2MeOH\}_\infty$ (4): $Mn(OAc)_2{\cdot}4H_2O$ (98 mg, 0.40 mmol) was dissolved in MeOH/DMF 4:1 (10 mL). A solution of tptz (125 mg, 0.40 mmol) in MeOH (10 mL) was added with stirring. The solution was layered with a solution of $[(C_4H_9)_4N]_4W(CN)_8$ (272 mg, 0.20 mmol) in MeOH (10 mL). Blue crystals were obtained after two weeks (166 mg, 66%). Elemental analysis (%) calcd for **4** ($WMn_2O_4N_{20}C_{48}H_{40}$): C 45.95, H 3.21, N 22.33; found: C 43.62, H 2.77, N 22.07; IR (Nujol): $\tilde{\nu}$ = 2098, 2111 cm^{-1} (C≡N).

$\{[Mn_2(tptz)_2(MeOH)_3(OAc)][W(CN)_8]{\cdot}3.5MeOH{\cdot}0.25H_2O\}_\infty$ (5): $Mn(OAc)_2{\cdot}4H_2O$ (98 mg, 0.40 mmol) was dried in vacuo for 10 h prior to use and then dissolved in anhydrous MeOH (8 mL). To this solution, a solution of tptz (125 mg, 0.40 mmol) in anhydrous MeOH (8 mL) was slowly added with constant stirring. The resulting dark yellow solution was layered in the dark with a solution of $[(C_4H_9)_3NH]_3W(CN)_8$ (190 mg, 0.20 mmol) in anhydrous MeOH (10 mL). Brown crystals were obtained after two weeks which were collected by filtration, washed with MeOH, and dried in vacuo (33 mg, 13%). Elemental analysis indicated that the interstitial solvent was lost when the sample was dried: elemental analysis calcd (%) for $[Mn_2(tptz)_2(MeOH)_3(OAc)][W(CN)_8]$ ($WMn_2O_5N_{20}C_{49}H_{39}$): C 45.92, H 3.07, N 21.86; found: C 43.95, H 2.89, N 21.80; IR (Nujol): $\tilde{\nu}$ = 2139, 2170, 2182 cm^{-1} (C≡N).

$[Mn_6(tptz)_6(MeOH)_4(DMF)_2W_4(CN)_{32}]{\cdot}8.2H_2O{\cdot}2.3MeOH$ (6): Compound **1** (73 mg, 0.15 mmol) was dissolved in MeOH/H_2O 4:1 (10 mL). This solution was layered in dark with a solution of $[(C_4H_9)_3NH]_3W(CN)_8$ (95 mg, 0.10 mmol) in MeOH (8 mL). Brown crystals obtained after two weeks were collected by filtration, washed with MeOH, and dried in vacuo (32 mg, 30%). Elemental analysis indicated that the interstitial methanol molecules were lost when the sample was dried: elemental analysis calcd (%) for $[Mn_6(tptz)_6(MeOH)_4(DMF)_2W_4(CN)_{32}]{\cdot}8.2H_2O$ ($W_4Mn_6O_{18.2}N_{68}C_{148}H_{124.4}$): C 42.21, H 2.98, N 22.61; found: C 41.70, H 2.69, N 22.75; IR (Nujol): $\tilde{\nu}$ = 2145, 2161, 2172, 2184 cm^{-1} (C≡N).

$\{[Mn_2(tptz)_2(MeOH)_3W(CN)_8][Mn(tptz)(MeOH)W(CN)_8]{\cdot}2H_2O{\cdot}MeOH\}_8$ (7): A quantity of **1** (73 mg, 0.15 mmol) was dissolved in anhydrous MeOH/DMF 4:1 (25 mL). The solution was stirred for 30 minutes and filtered. The filtrate was layered in the dark with a solution of $[(C_4H_9)_3NH]_3W(CN)_8$ (95 mg, 0.10 mmol) in anhydrous MeOH (10 mL). Brown crystals that grew over the course of one week were collected by filtration, washed with MeOH and dried in vacuo (24 mg, 24%). Elemental analysis indicated that the interstitial solvent was lost when the sample was dried: elemental analysis calcd (%) for $\{[Mn_2(tptz)_2(MeOH)_3W(CN)_8][Mn(tptz)(MeOH)W(CN)_8]\}_8$ ($W_2Mn_3O_4N_{34}C_{74}H_{52}$): C 44.13, H 2.60, N 23.65; found: C 43.05, H 2.41, N 23.75; IR (Nujol): $\tilde{\nu}$ = 2143, 2162, 2173 cm^{-1} (C≡N).

$[Mn(tptz)(MeOH)(NO_3)]_2[Mn(tptz)(MeOH)(DMF)]_2[W(CN)_8]_2{\cdot}6MeOH$ (8): A sample of **2** (83 mg, 0.15 mmol) was dissolved in MeOH/H_2O 3:2 (10 mL). This solution was layered in the dark with a solution of $[(C_4H_9)_3NH]_3W(CN)_8$ (95 mg, 0.10 mmol) in MeOH (10 mL). Yellow crystals that formed after two days were collected by filtration, washed with MeOH, and dried in vacuo (28 mg, 21%). Elemental analysis indicated that the interstitial solvent was lost when the sample was dried: elemental analysis calcd (%) for $[Mn(tptz)(MeOH)(NO_3)]_2[Mn(tptz)(MeOH)(DMF)]_2[W(CN)_8]_2$ ($W_2Mn_4O_{12}N_{44}C_{98}H_{78}$): C 44.39, H 2.97, N 23.24; found: C 42.06, H 2.82, N, 22.52; IR (Nujol): $\tilde{\nu}$ = 2148, 2161, 2187 cm^{-1} (C≡N).

Physical measurements: IR spectra of compounds **3**–**8** were measured as Nujol mulls placed between KBr plates on a Nicolet 740 FT-IR spectrometer. Magnetic susceptibility and magnetization measurements were carried out with a Quantum Design SQUID magnetometer MPMS-XL. DC magnetic measurements were performed in an applied field of 1000 Oe in a temperature range of 2–300 K. AC magnetic susceptibility measurements were performed in a 3 Oe AC field in an operating frequency range of 1–1000 Hz. Magnetization data were collected at 1.8 K in the 0–7 T range starting at zero field. The molecular weight of the compounds was adjusted according to the results of elemental analysis. The data were corrected for diamagnetic contributions calculated from the Pascal constants.[45]

Single crystal X-ray diffraction studies: In a typical experiment, a crystal selected for study was suspended in Paratone oil and mounted on a cryoloop which was placed in an N_2 cold stream. Single crystal X-ray data were collected on a Bruker APEX (**1**, **2**, **7**, and **8**) and a Bruker SMART 1000 (**3**–**6**) diffractometers equipped with a CCD detector, at temperatures between 110 and 150 K (Table 2). The data sets were recorded as ω scans at 0.3° step width and integrated with the Bruker SAINT[46] soft-

ware package. The absorption correction (SADABS[47]) was based on fitting a function to the empirical transmission surface as sampled by multiple equivalent measurements. Solution and refinement of the crystal structures was carried out using the SHELX[48] suite of programs and the graphical interface X-SEED.[49] All the structures were solved by direct methods which resolved the positions of all metal atoms and most of C and N atoms. The remaining non-hydrogen atoms were located by alternating cycles of least squares refinements and difference Fourier maps. Hydrogen atoms were placed at calculated positions, with the exception of some water molecules, for which hydrogen atoms were located by the difference Fourier maps. Whenever disordered solvent molecules were present in a structure, their bond lengths were restrained to chemically meaningful values. The final refinement was carried out with anisotropic thermal parameters for all non-hydrogen atoms, except for the non-hydrogen atoms of the disordered solvent molecules which were refined isotropically. A summary of pertinent information relating to unit cell parameters, data collection, and refinement statistics is provided in Table 2.

CCDC-637 310–637 317 contain the supplementary crystallographic data for this paper. These data can be obtained free of charge from The Cambridge Crystallographic Data Centre via www.ccdc.cam.ac.uk/data_request/cif.

Acknowledgement

This research was supported by Department of Energy (PI grant DE-FG01-05ER05-01) and the Robert Welch Foundation (grant A-1449). Funding of the CCD diffractometer (grant 9807975) and SQUID magnetometer (grant 9974899) by NSF is gratefully acknowledged. We also thank Texas A&M Supercomputing Facility for providing computer time.

[1] T. Mallah, S. Thiebaut, M. Verdaguer, P. Veillet, *Science* **1993**, *262*, 1554–1557.
[2] W. R. Entley, G. Girolami, *Science* **1995**, *268*, 397–400.
[3] S. M. Holmes, G. Girolami, *J. Am. Chem. Soc.* **1999**, *121*, 5593–5594.
[4] K. R. Dunbar, R. A. Heintz, *Prog. Inorg. Chem.* **1997**, *45*, 283–391.
[5] O. Sato, T. Iyoda, A. Fujishima, K. Hashimoto, *Science* **1996**, *272*, 704–705.
[6] J. M. Herrera, V. Marvaud, M. Verdaguer, J. Marrot, M. Kalisz, C. Mathonière, *Angew. Chem.* **2004**, *116*, 5584–5587; *Angew. Chem. Int. Ed.* **2004**, *43*, 5468–5471.
[7] J. J. Sokol, A. G. Hee, J. R. Long, *J. Am. Chem. Soc.* **2002**, *124*, 7656–7657.
[8] C. P. Berlinguette, D. Vaughn, C. Cañada-Vilalta, J. R. Galán-Mascarós, K. R. Dunbar, *Angew. Chem.* **2003**, *115*, 1561–1564; *Angew. Chem. Int. Ed.* **2003**, *42*, 1523–1526.
[9] H. J. Choi, J. J. Sokol, J. R. Long, *Inorg. Chem.* **2004**, *43*, 1606–1608.
[10] E. J. Schelter, A. V. Prosvirin, K. R. Dunbar, *J. Am. Chem. Soc.* **2004**, *126*, 15004–15005.
[11] S. Wang, J. L. Zuo, H. C. Zhou, H. J. Choi, Y. Ke, J. R. Long, X. Z. You, *Angew. Chem.* **2004**, *116*, 6066–6069; *Angew. Chem. Int. Ed.* **2004**, *43*, 5940–5943.
[12] D. Li, S. Parkin, G. Wang, G. T. Yee, A. V. Prosvirin, S. M. Holmes, *Inorg. Chem.* **2005**, *44*, 4903–4905.
[13] Y. Song, P. Zhang, X. M. Ren, X. F. Shen, Y. Z. Li, X. Z. You, *J. Am. Chem. Soc.* **2005**, *127*, 3708–3709.
[14] S. Bonhommeau, G. Molnár, A. Galet, A. Zwick, J. A. Real, J. J. McGarvey, A. Bousseksou, *Angew. Chem.* **2005**, *117*, 4137–4141; *Angew. Chem. Int. Ed.* **2005**, *44*, 4069–4073.
[15] E. Coronado, M. C. Giménez-López, G. Levchenko, F. M. Romero, V. García-Baonza, A. Milner, M. Paz-Pasternak, *J. Am. Chem. Soc.* **2005**, *127*, 4580–4581.
[16] W. Kosaka, K. Nomura, K. Hashimoto, S. Ohkoshi, *J. Am. Chem. Soc.* **2005**, *127*, 8590–8591.
[17] M. Shatruk, K. Chambers, A. Dragulescu-Andrasi, S. A. Stoian, E. A. Bominaar, C. Achim, K. R. Dunbar, *J. Am. Chem. Soc.* **2007**, *129*, 6104–6116.
[18] C. P. Berlinguette, A. Dragulescu-Andrasi, A. Sieber, J. R. Galán-Mascarós, H. U. Güdel, C. Achim, K. R. Dunbar, *J. Am. Chem. Soc.* **2004**, *126*, 6222–6223.
[19] C. P. Berlinguette, A. Dragulescu-Andrasi, A. Sieber, H. U. Güdel, C. Achim, K. R. Dunbar, *J. Am. Chem. Soc.* **2005**, *127*, 6766–6779.
[20] E. L. Muetterties, *Inorg. Chem.* **1973**, *12*, 1963–1966.
[21] J. K. Burdett, R. Hoffmann, R. C. Fay, *Inorg. Chem.* **1978**, *17*, 2553–2568.
[22] J. Larionova, M. Gross, M. Pilkington, H. Andres, H. Stoeckli-Evans, H. U. Güdel, S. Decurtins, *Angew. Chem.* **2000**, *112*, 1667–1672; *Angew. Chem. Int. Ed.* **2000**, *39*, 1605–1609.
[23] Z. J. Zhong, H. Seino, Y. Mizobe, M. Hidai, A. Fujishima, S. i. Ohkoshi, K. Hashimoto, *J. Am. Chem. Soc.* **2000**, *122*, 2952–2953.
[24] F. Bonadio, M. Gross, H. Stoeckli-Evans, S. Decurtins, *Inorg. Chem.* **2002**, *41*, 5891–5896.
[25] J. H. Lim, J. H. Yoon, H. C. Kim, C. S. Hong, *Angew. Chem.* **2006**, *118*, 7584–7586; *Angew. Chem. Int. Ed.* **2006**, *45*, 7424–7426.
[26] B. Sieklucka, R. Podgajny, P. Przychodzen, T. Korzeniak, *Coord. Chem. Rev.* **2005**, *249*, 2203–2221.
[27] P. Przychodzen, T. Korzeniak, R. Podgajny, B. Sieklucka, *Coord. Chem. Rev.* **2006**, *250*, 2234–2260.
[28] R. Lescouëzec, J. Vaissermann, L. M. Toma, R. Carrasco, F. Lloret, M. Julve, *Inorg. Chem.* **2004**, *43*, 2234–2236.
[29] R. Kania, K. Lewinski, B. Sieklucka, *Dalton Trans.* **2003**, 1033–1040.
[30] R. Podgajny, T. Korzeniak, K. Stadnicka, Y. Dromzée, N. W. Alcock, W. Errington, K. Kruczała, M. Bałanda, T. J. Kemp, M. Verdaguer, B. Sieklucka, *Dalton Trans.* **2003**, 3458–3468.
[31] D. F. Li, S. Gao, L. M. Zheng, W. X. Tang, *J. Chem. Soc. Dalton Trans.* **2002**, 2805–2806.
[32] D. Li, L. Zheng, Y. Zhang, J. Huang, S. Gao, W. Tang, *Inorg. Chem.* **2003**, *42*, 6123–6129.
[33] G. Rombaut, S. Golhen, L. Ouahab, C. Mathonière, O. Kahn, *Dalton* **2000**, 3609–3614.
[34] M. A. Porai-Koshits, L. A. Aslanov, *Zh. Strukt. Khim.* **1972**, *13*, 266–276.
[35] L. D. C. Bok, J. G. Leipoldt, S. S. Basson, *Acta Crystallogr. Sect. B* **1970**, *26*, 684–692.
[36] J. Kim, S. Han, K. I. Pokhodnya, J. M. Migliori, J. S. Miller, *Inorg. Chem.* **2005**, *44*, 6983–6988.
[37] J. J. Borrás-Almenar, J. M. Clemente-Juan, E. Coronado, B. S. Tsukerblat, *J. Comput. Chem.* **2001**, *22*, 985–991.
[38] R. Podgajny, C. Desplanches, B. Sieklucka, R. Sessoli, V. Villar, C. Paulsen, W. Wernsdorfer, Y. Dromzée, M. Verdaguer, *Inorg. Chem.* **2002**, *41*, 1323–1327.
[39] Y. Pei, O. Kahn, J. Sletten, J. P. Renard, R. Georges, J. C. Gianduzzo, J. Curely, Q. Xu, *Inorg. Chem.* **1988**, *27*, 47–53.
[40] R. Georges, J. Curely, J. C. Gianduzzo, Q. Wu, O. Kahn, Y. Pei, *Phys. B* **1988**, *153*, 77–84.
[41] M. Drillon, E. Coronado, R. Georges, J. C. Gianduzzo, J. Curely, *Phys. Rev. B* **1989**, *40*, 10992–10998.
[42] D. Gatteschi, R. Sessoli, *Angew. Chem.* **2003**, *115*, 278–309; *Angew. Chem. Int. Ed.* **2003**, *42*, 268–297.
[43] R. Schenker, M. N. Leuenberger, G. Chaboussant, D. Loss, H. U. Güdel, *Phys. Rev. B* **2005**, *72*, 184403.
[44] L. D. C. Bok, J. G. Leipoldt, S. S. Basson, *Z. Anorg. Allg. Chem.* **1975**, *415*, 81–83.
[45] R. L. Carlin, *Magnetochemistry*, Springer, Heidelberg, **1986**.
[46] SMART and SAINT, Siemens Analytical X-ray Instruments Inc., Madison, WI (USA), **1996**.
[47] G. M. Sheldrick, SADABS, University of Göttingen, Göttingen (Germany), **1996**.
[48] G. M. Sheldrick, SHELXS-97 and SHELXL-97, University of Göttingen, Göttingen (Germany), **1997**.
[49] L. J. Barbour, *J. Supramol. Chem.* **2001**, *1*, 189–191.

Received: February 21, 2007
Published online: June 14, 2007

